Electronic Supplementary Material (ESI) for New Journal of Chemistry.


# Synthesis, characterization and bioactivity studies of new dithiocarbazate complexes

Zahra Yekke-ghasemi,[a] Mohamad Ramezani,[b] Joel T. Mague[c] and Reza Takjoo,*[a]

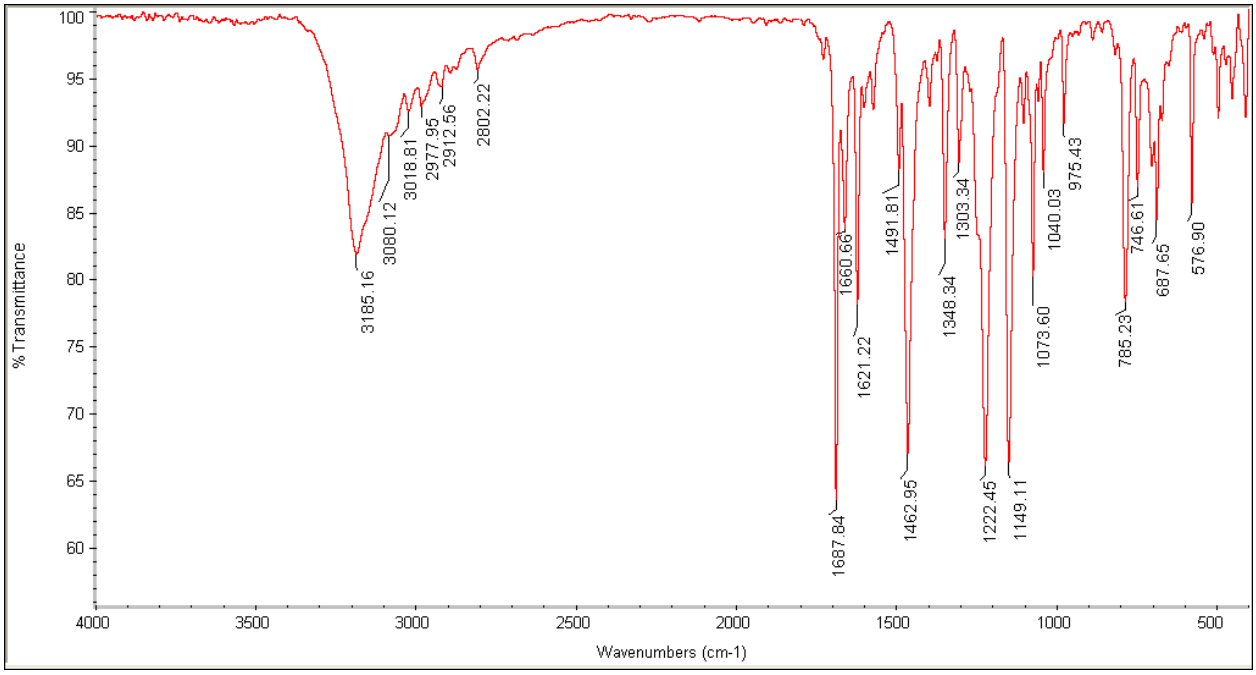


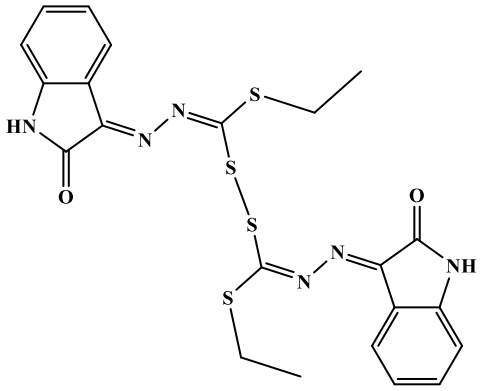


SI 1a. IR spectrum of L.

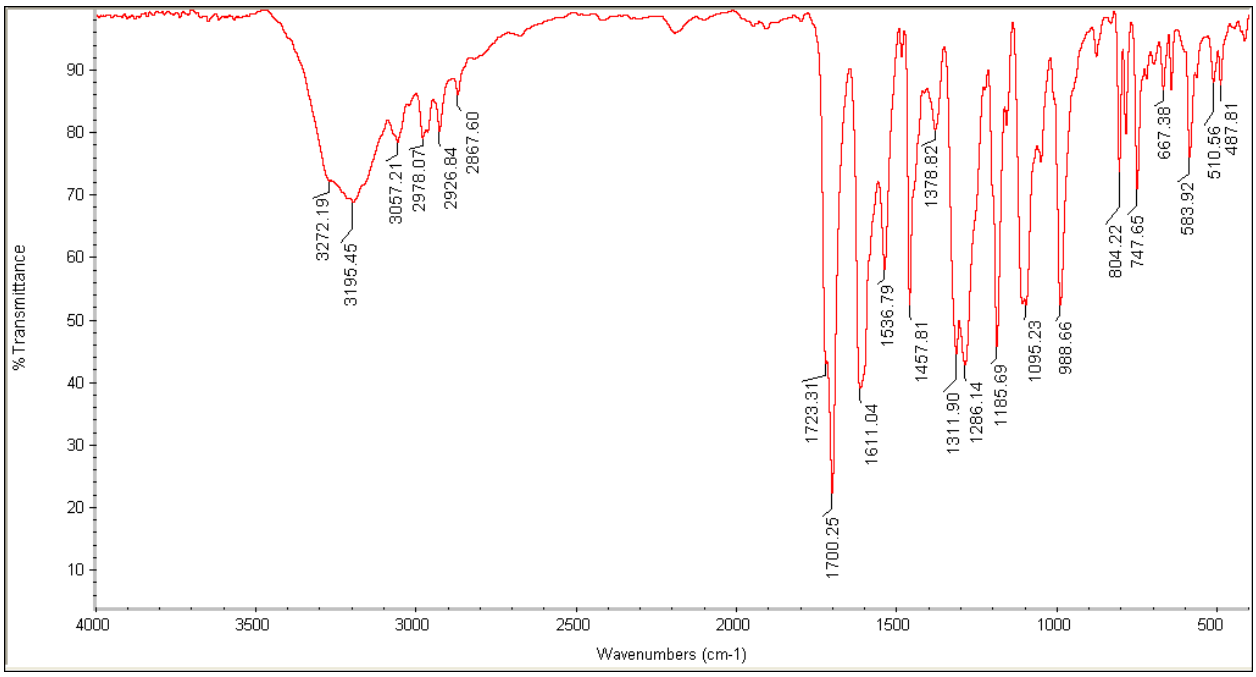


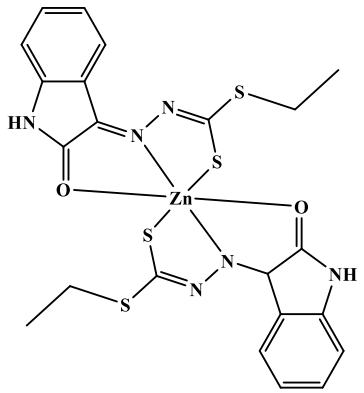


SI 1b. IR spectrum of **1**.

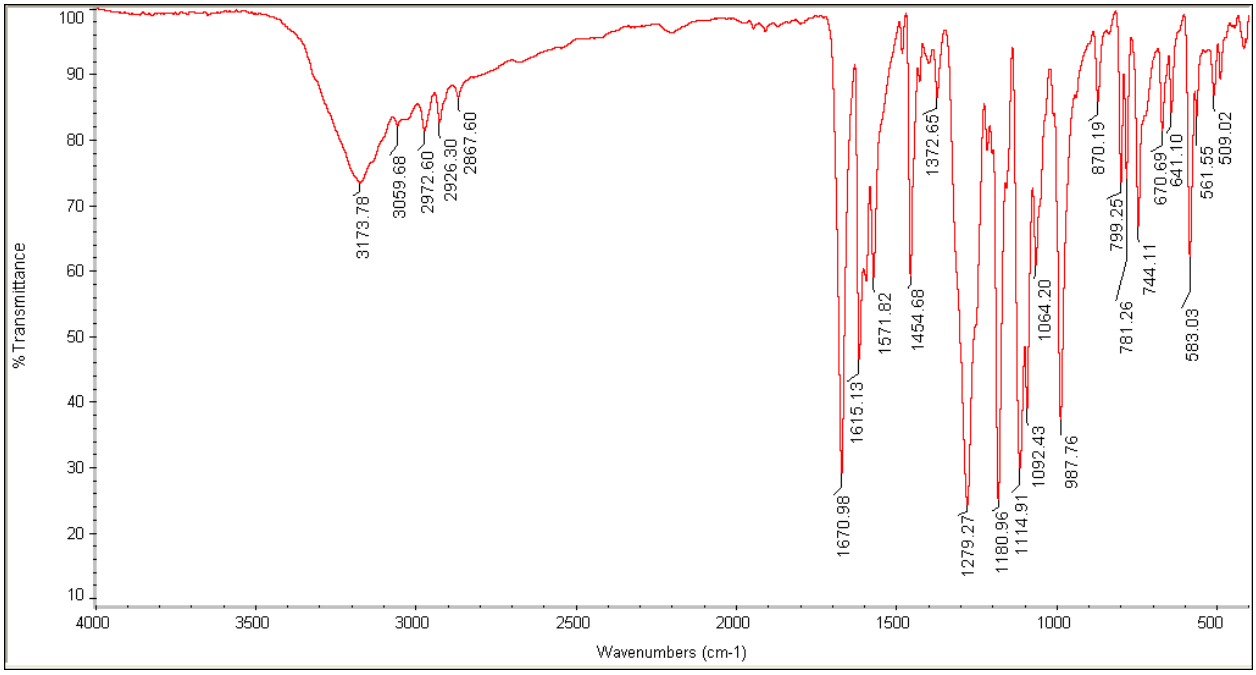


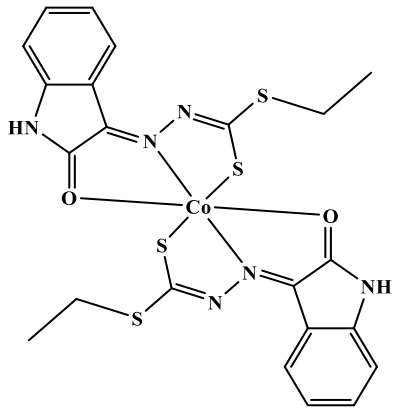


SI 1c. IR spectrum of **2**.

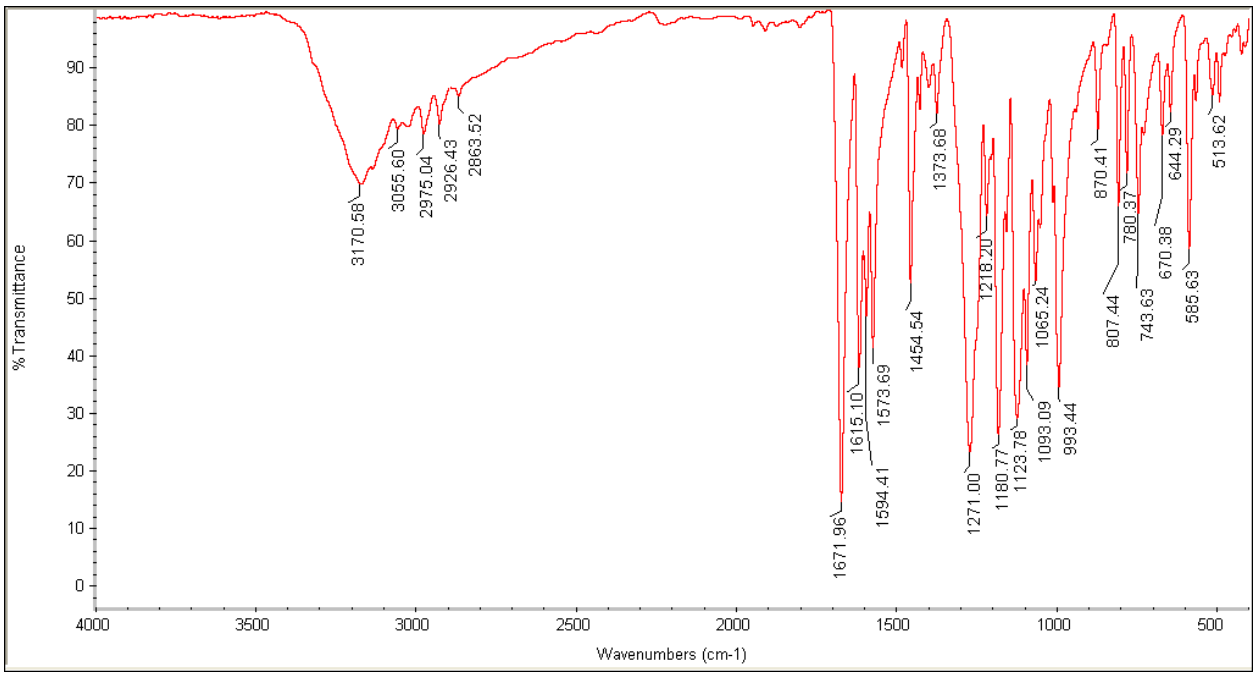


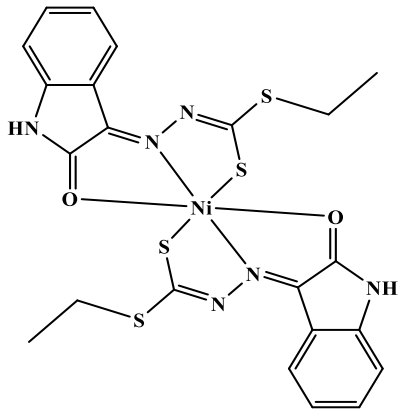


SI 1d. IR spectrum of **3**.

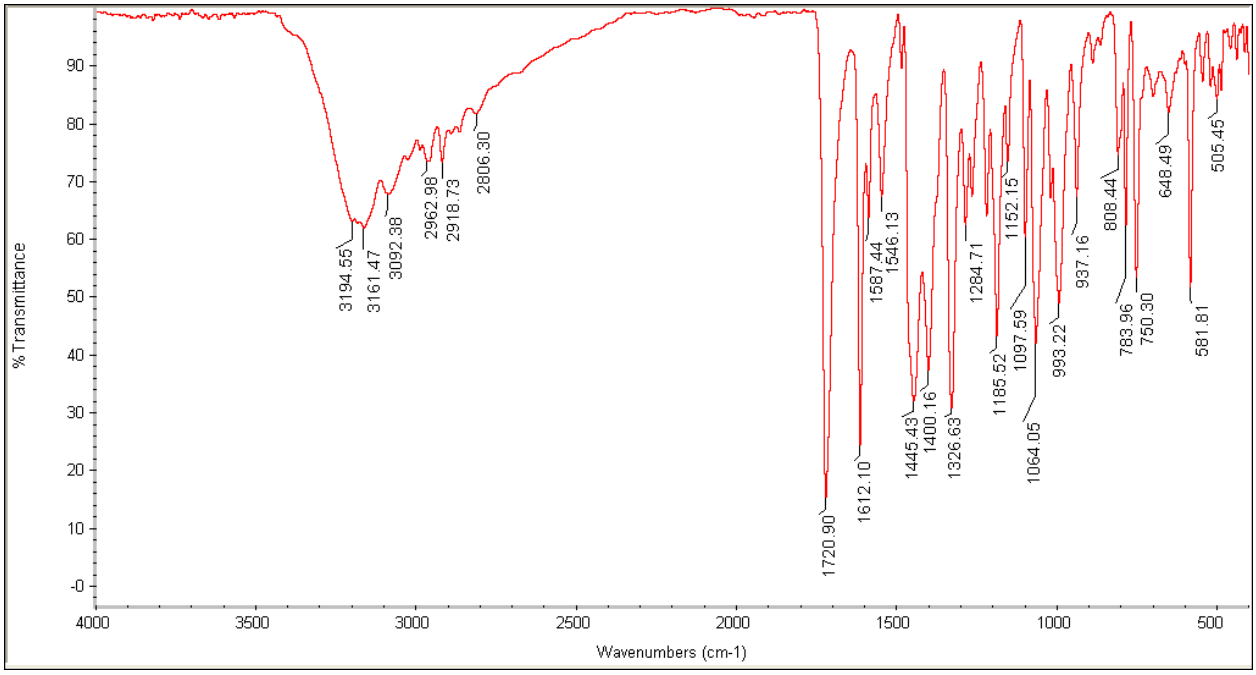


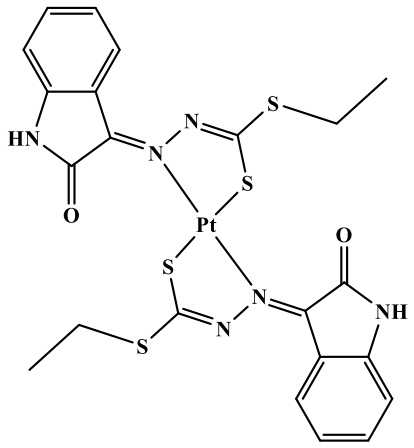


SI 1e. IR spectrum of **4**.

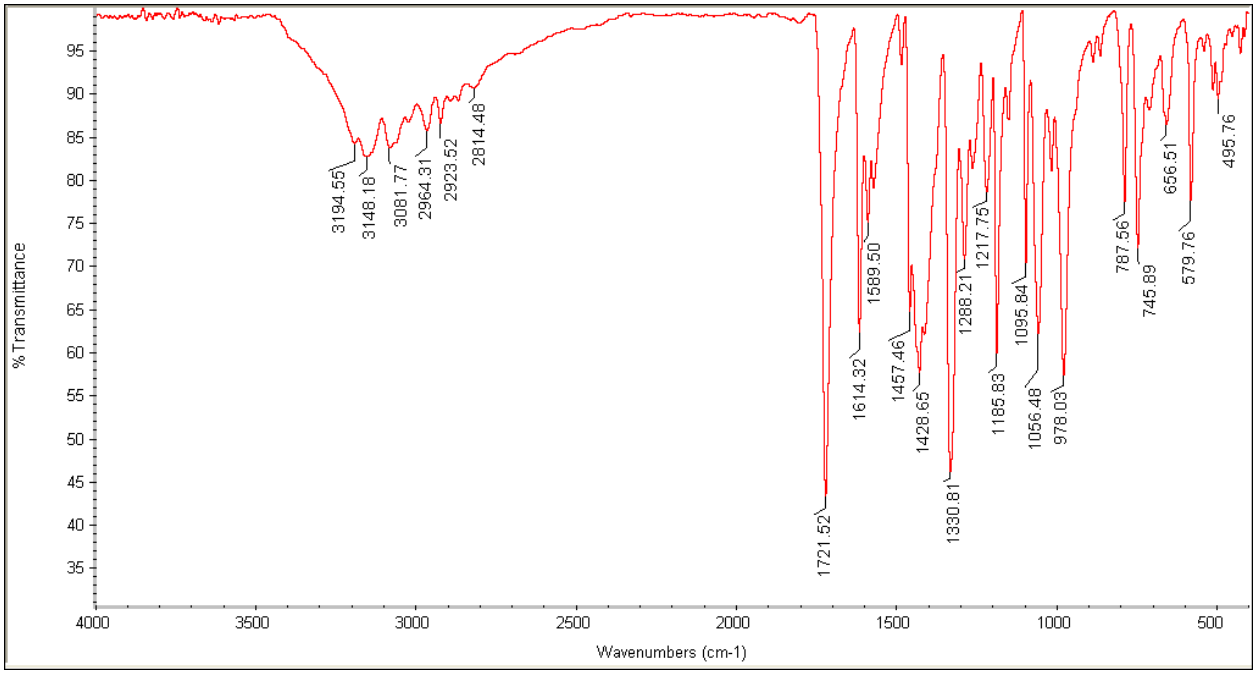


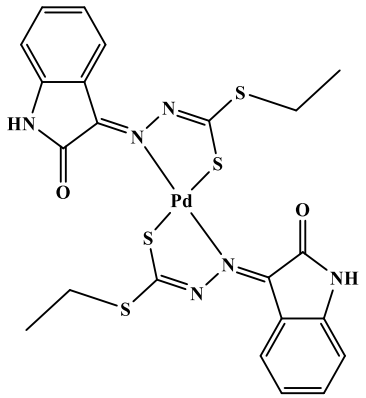


SI 1f. IR spectrum of **5**.

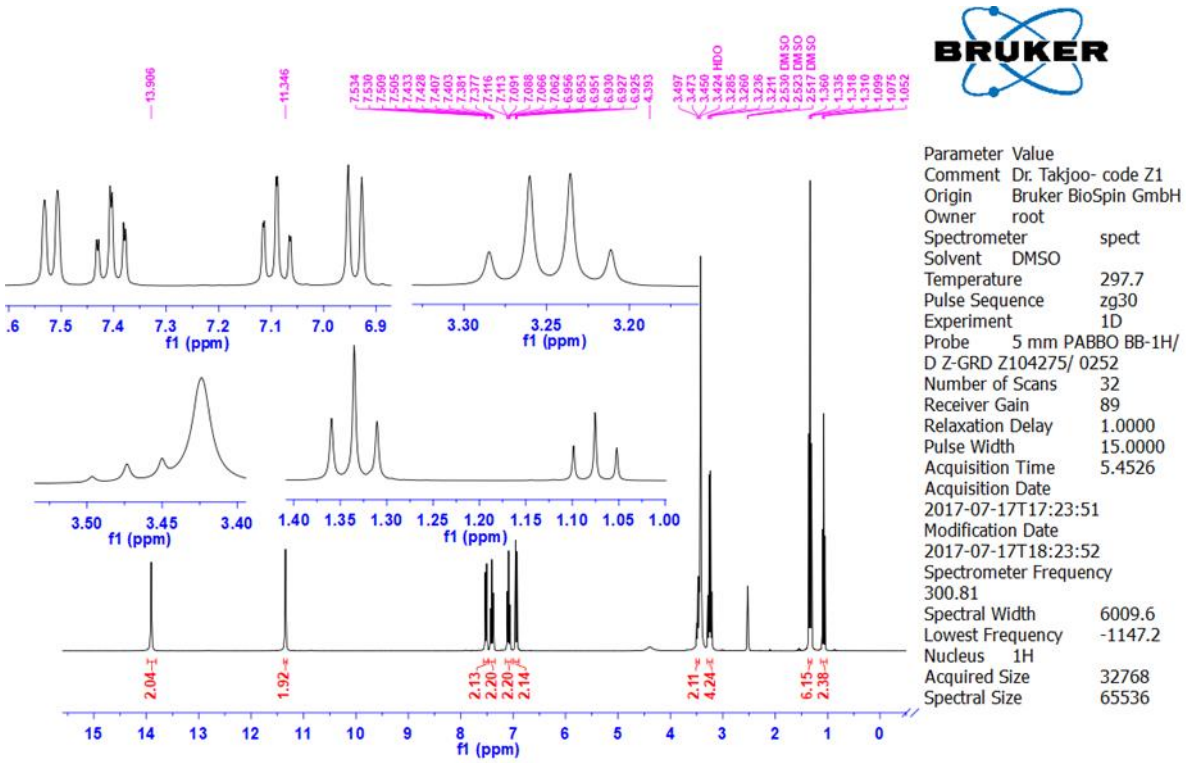


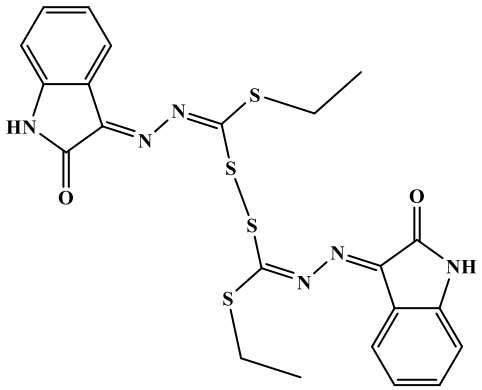


SI 2a. $^{1}$HNMR spectrum of L in DMSO-$d_6$.

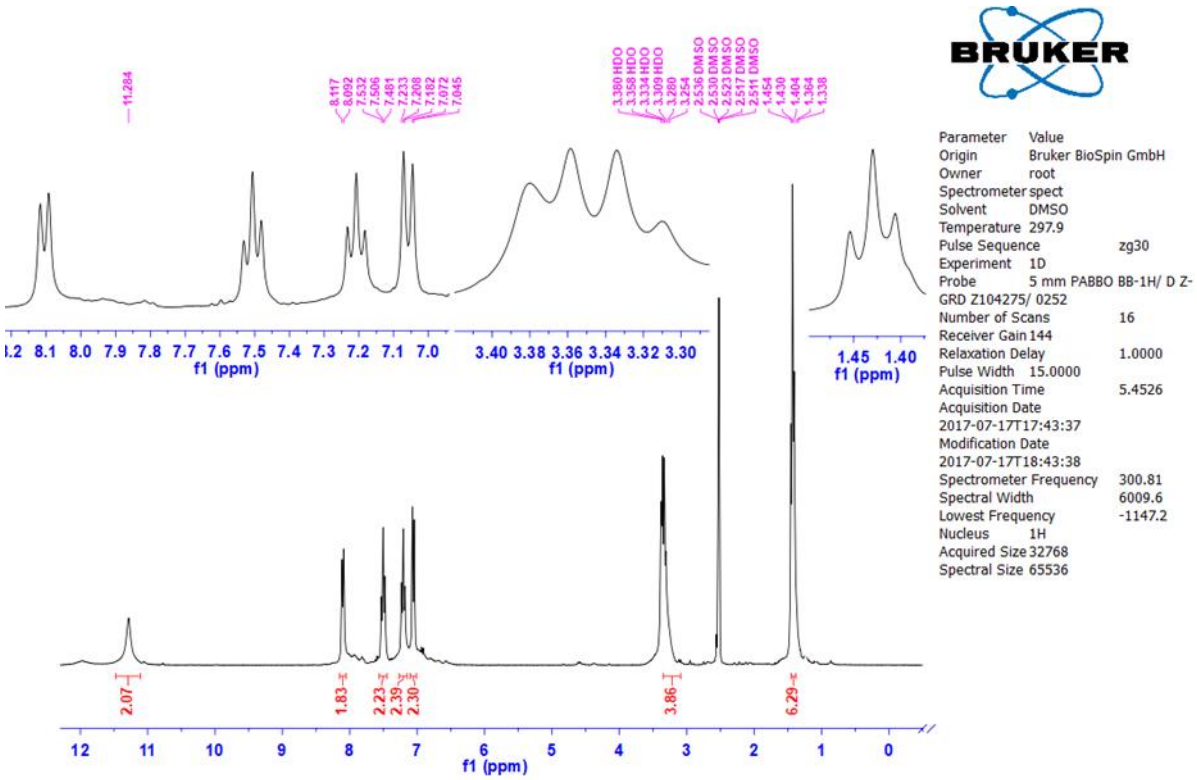


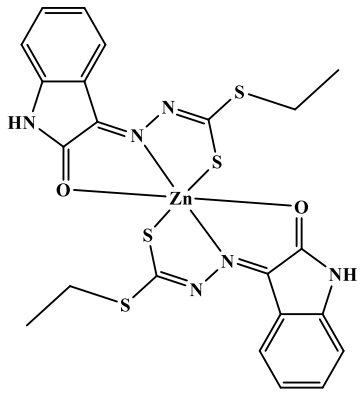


SI 2b. $^{1}$HNMR spectrum of **1** in DMSO-$d_6$.

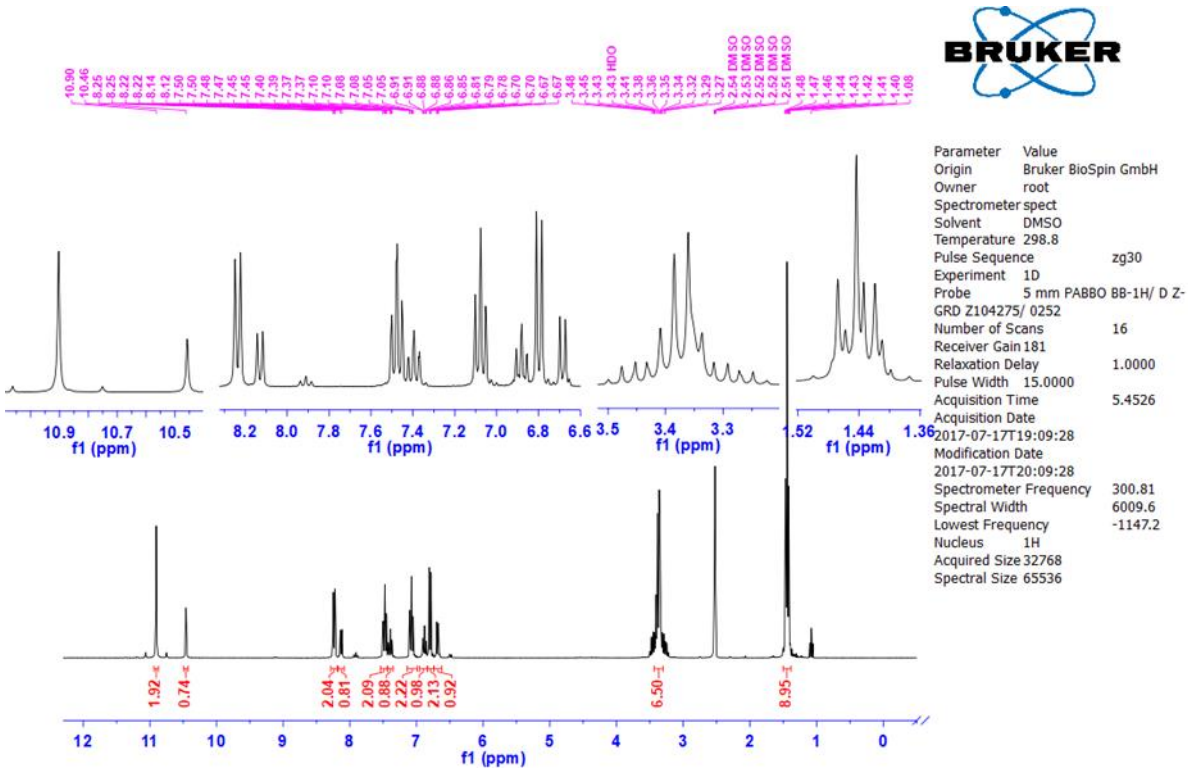


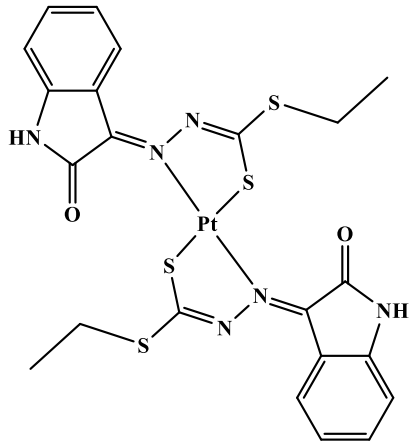


SI 2c. $^{1}$HNMR spectrum of **4** in DMSO-$d_6$.

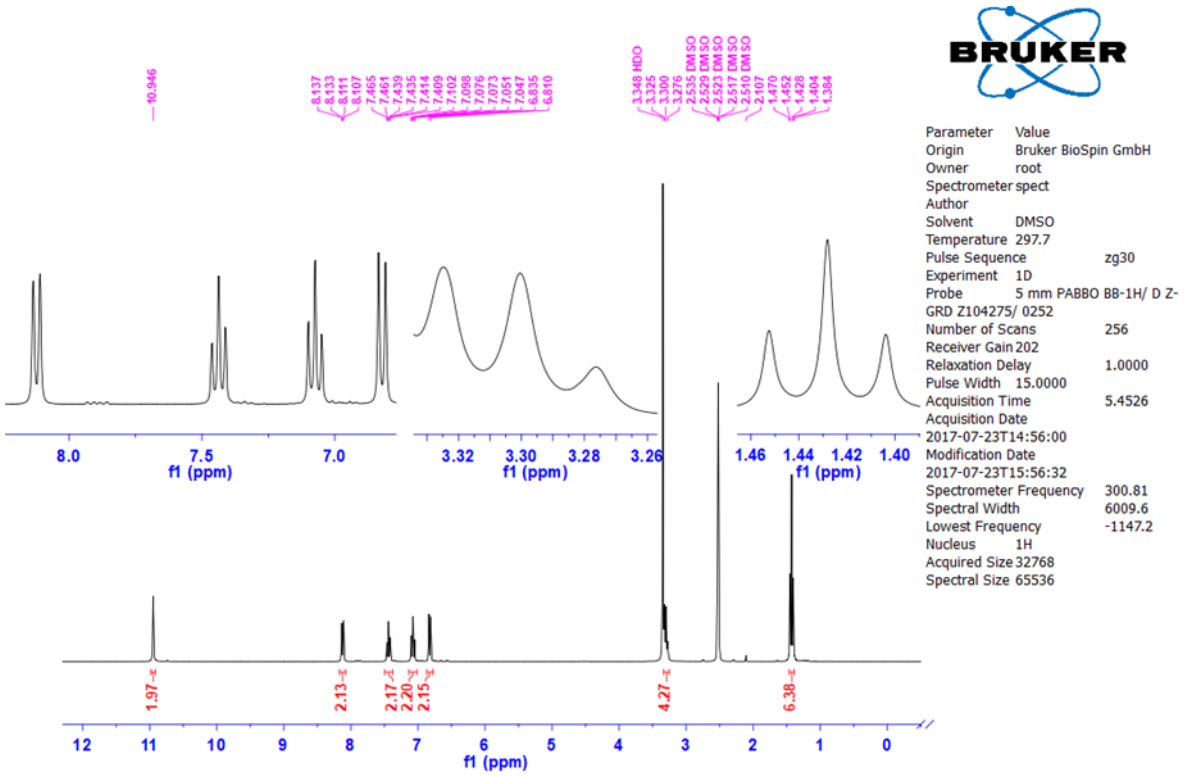


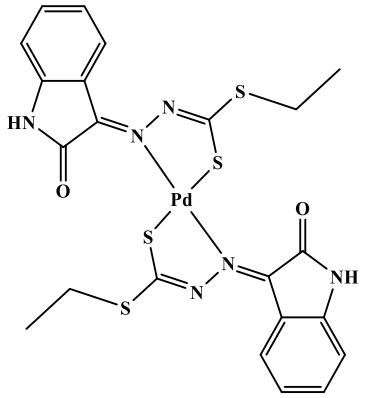


SI 2d. $^{1}$HNMR spectrum of **5** in DMSO-$d_6$.

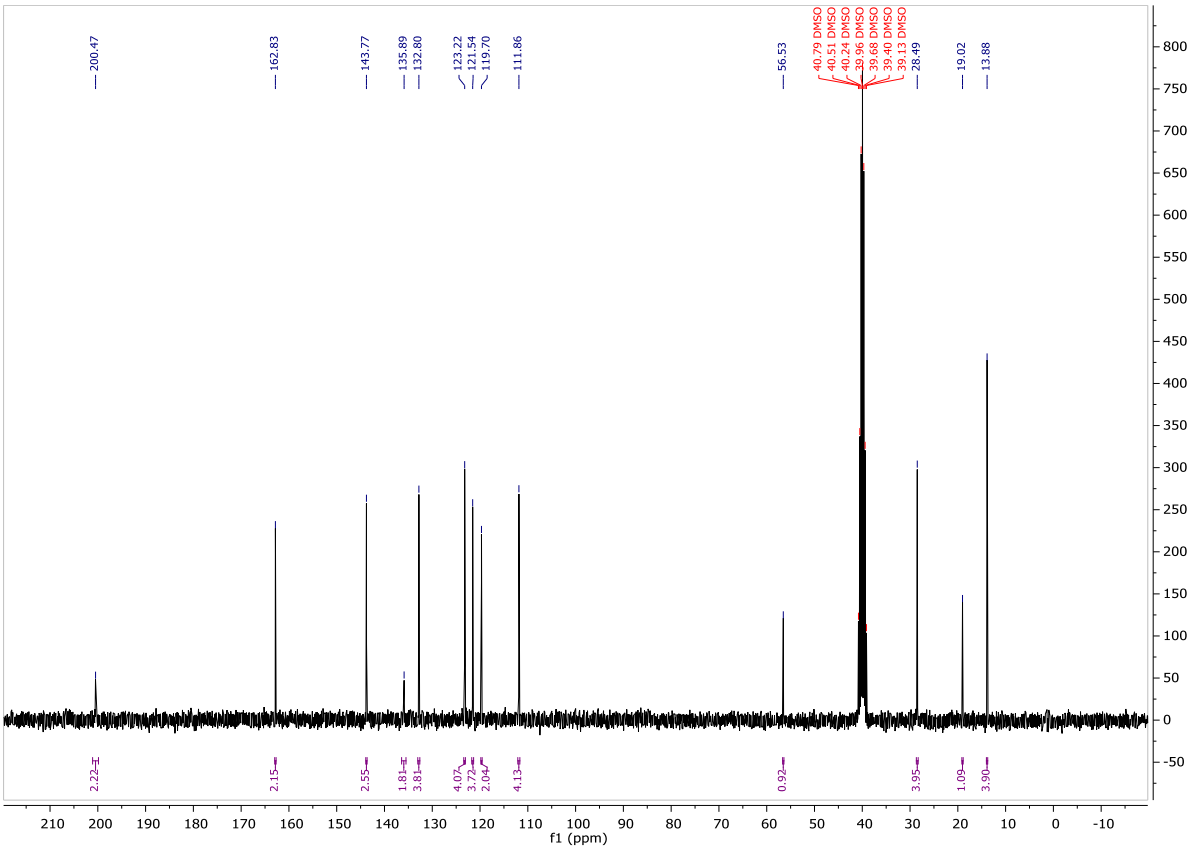


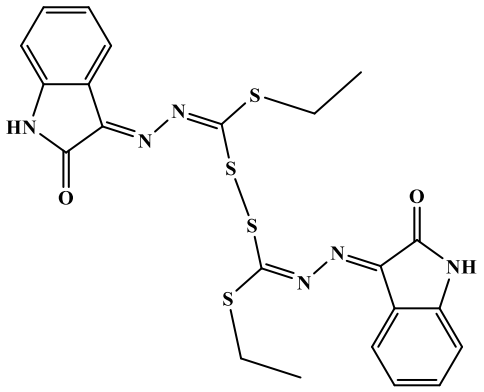


SI 3a. $^{13}$CNMR spectrum of **L** in DMSO-$d_6$.

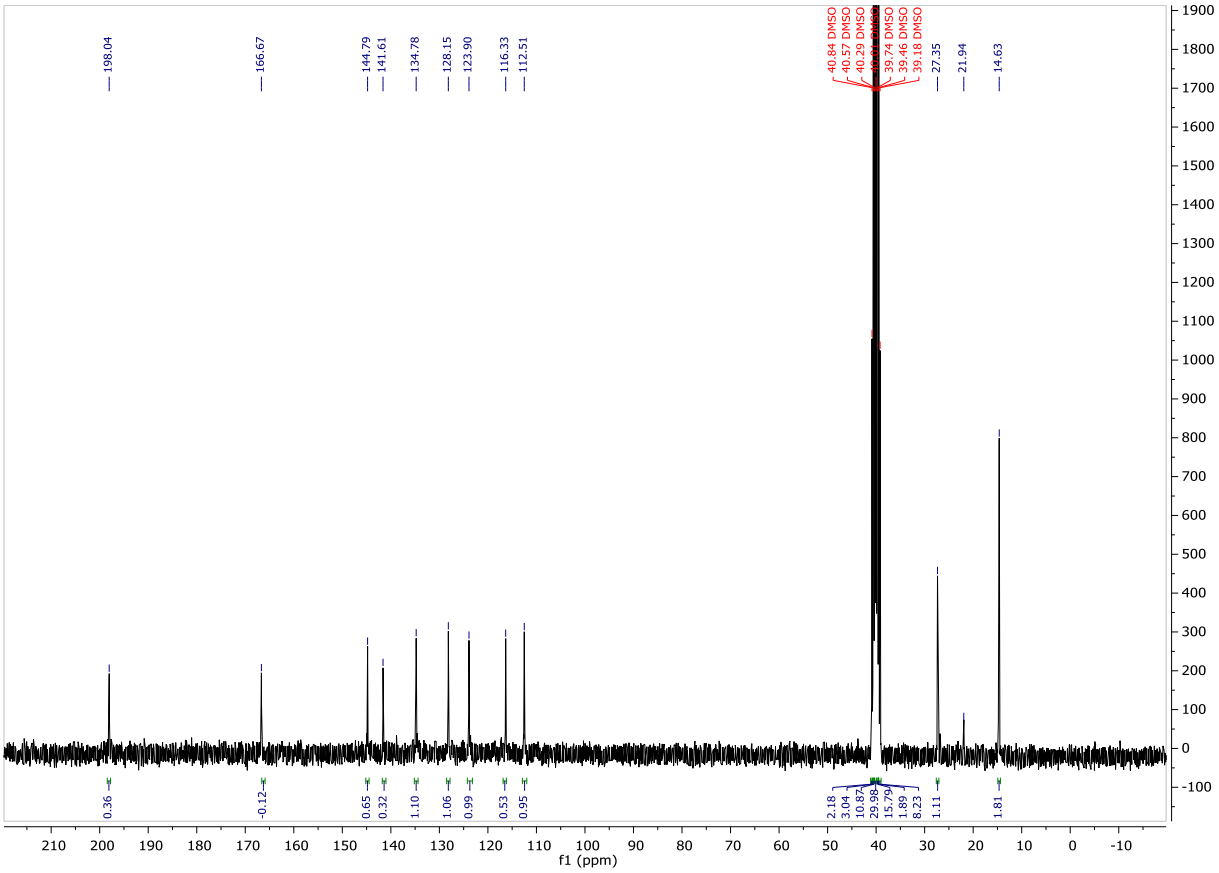


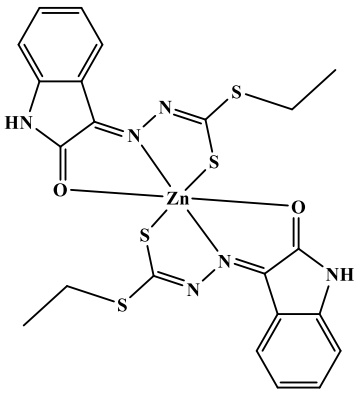


SI 3b. $^{13}$CNMR spectrum of **1** in DMSO-$d_6$.

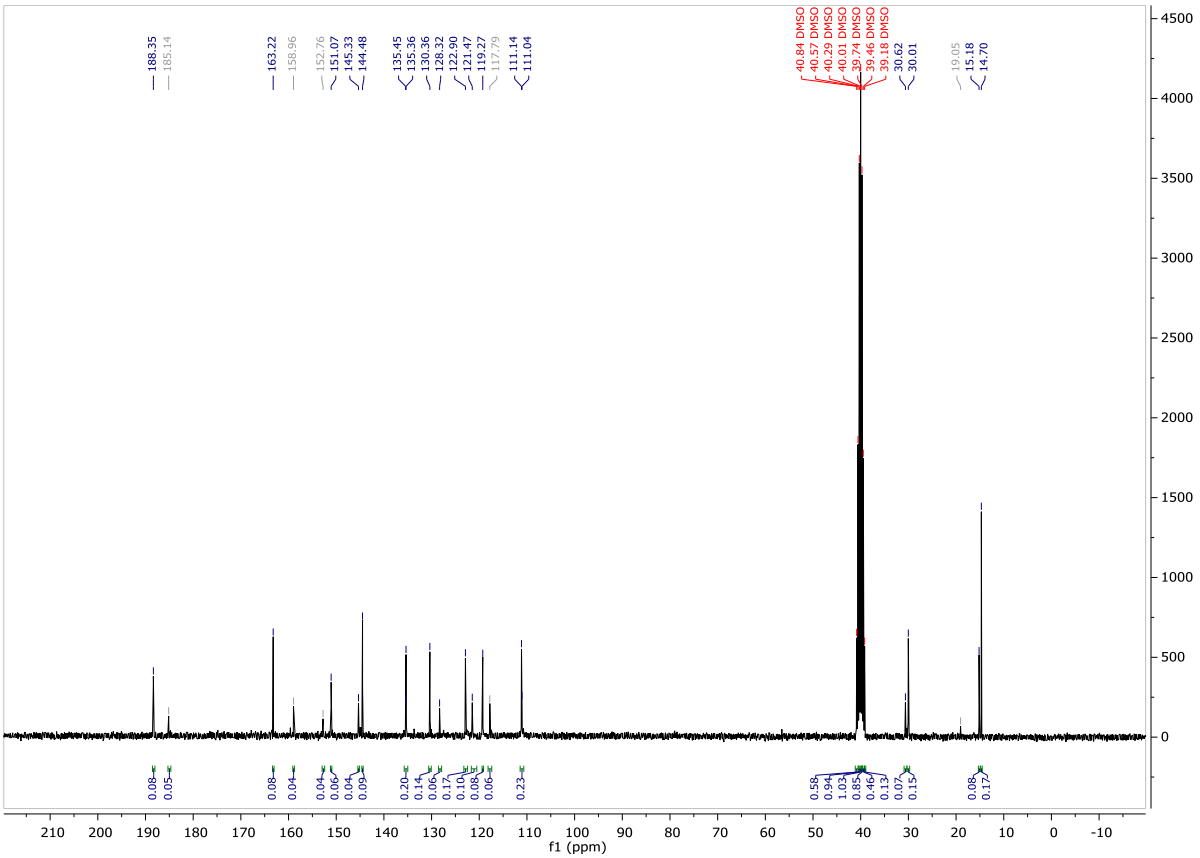


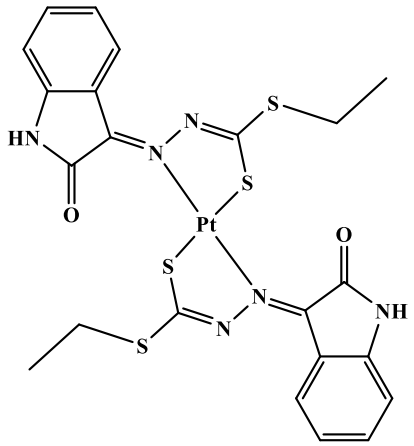


SI 3c. $^{13}$CNMR spectrum of **4** in DMSO-$d_6$.

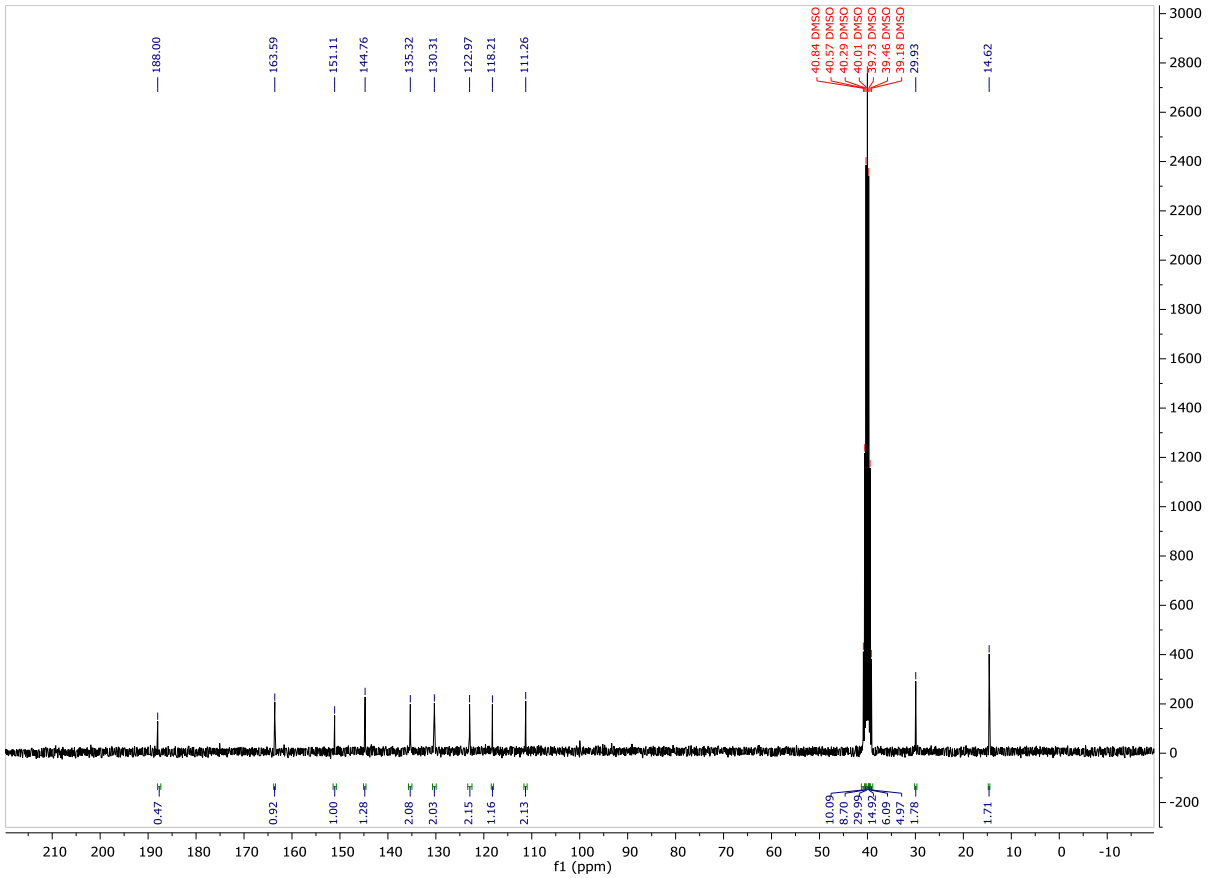


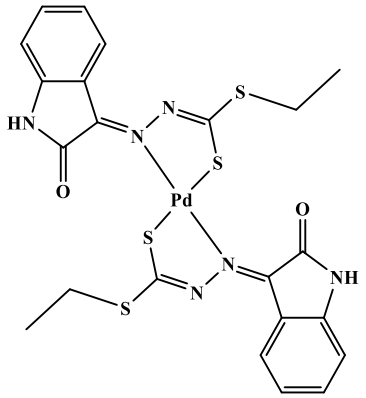


SI 3d. $^{13}$CNMR spectrum of **5** in DMSO-$d_6$.

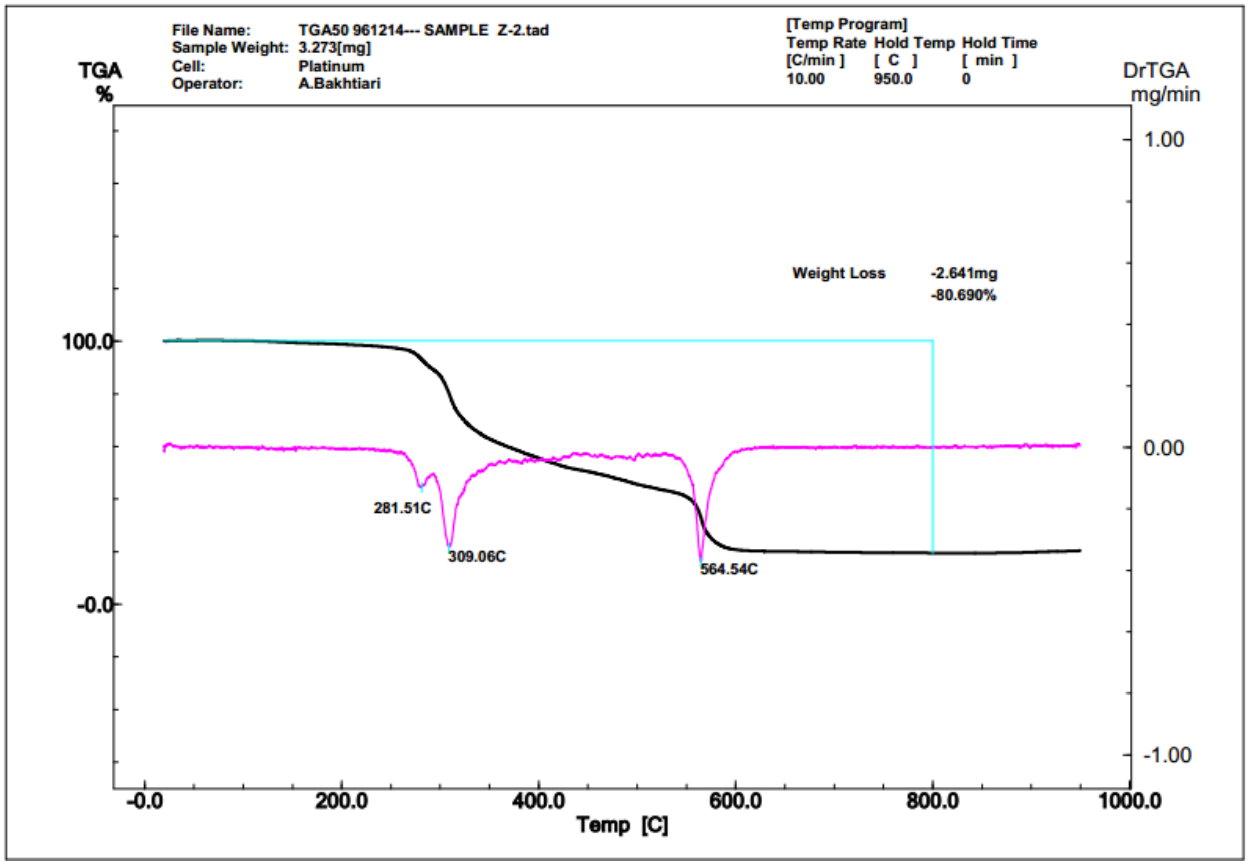


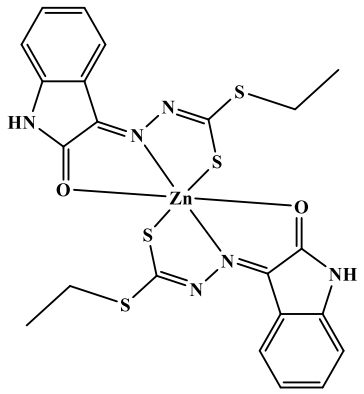


SI 4a. TGA and DTG curves thermogram of **1**.

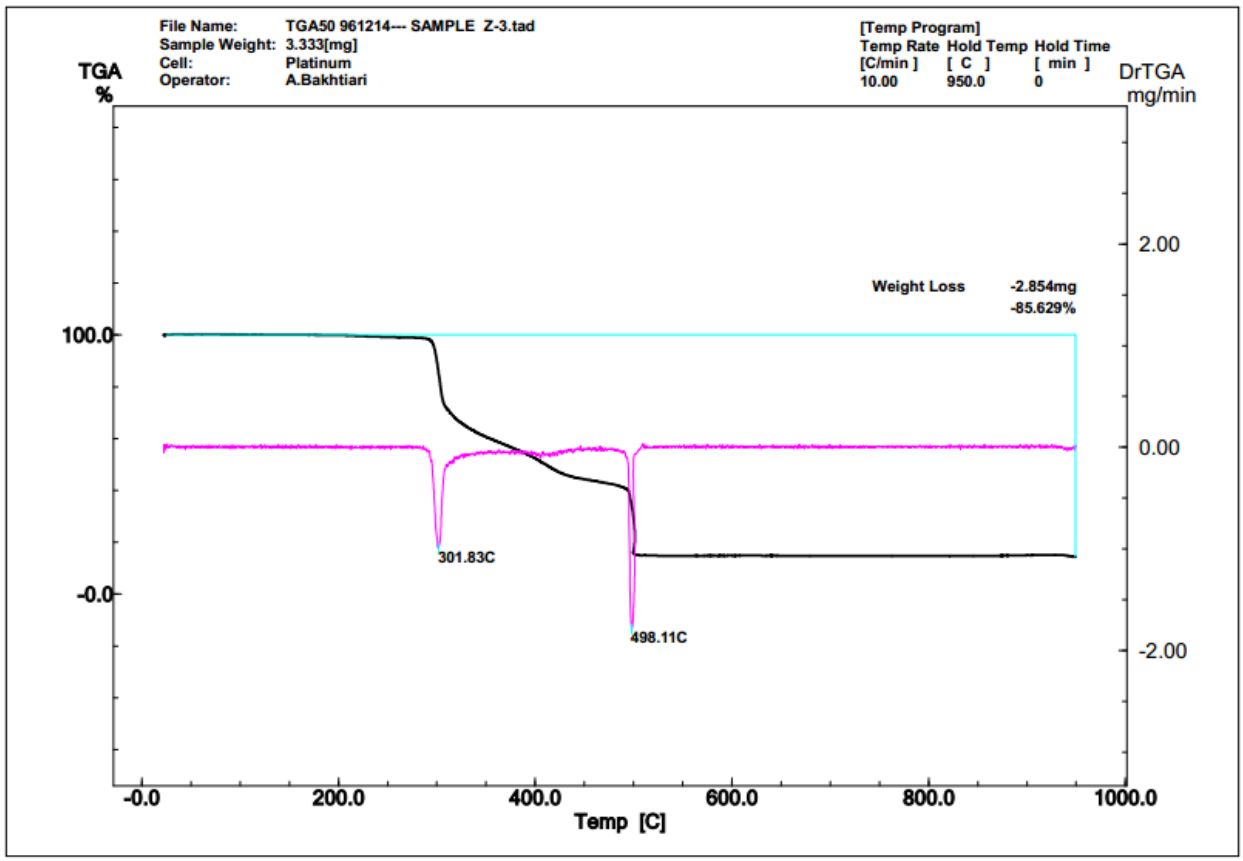


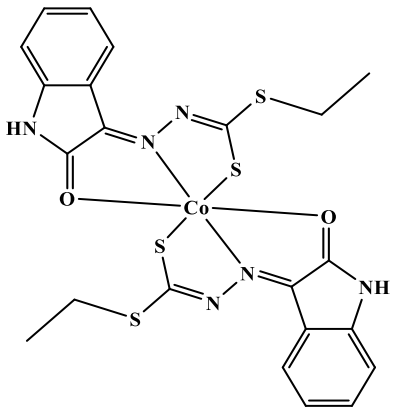


SI 4b. TGA and DTG curves thermogram of **2**.

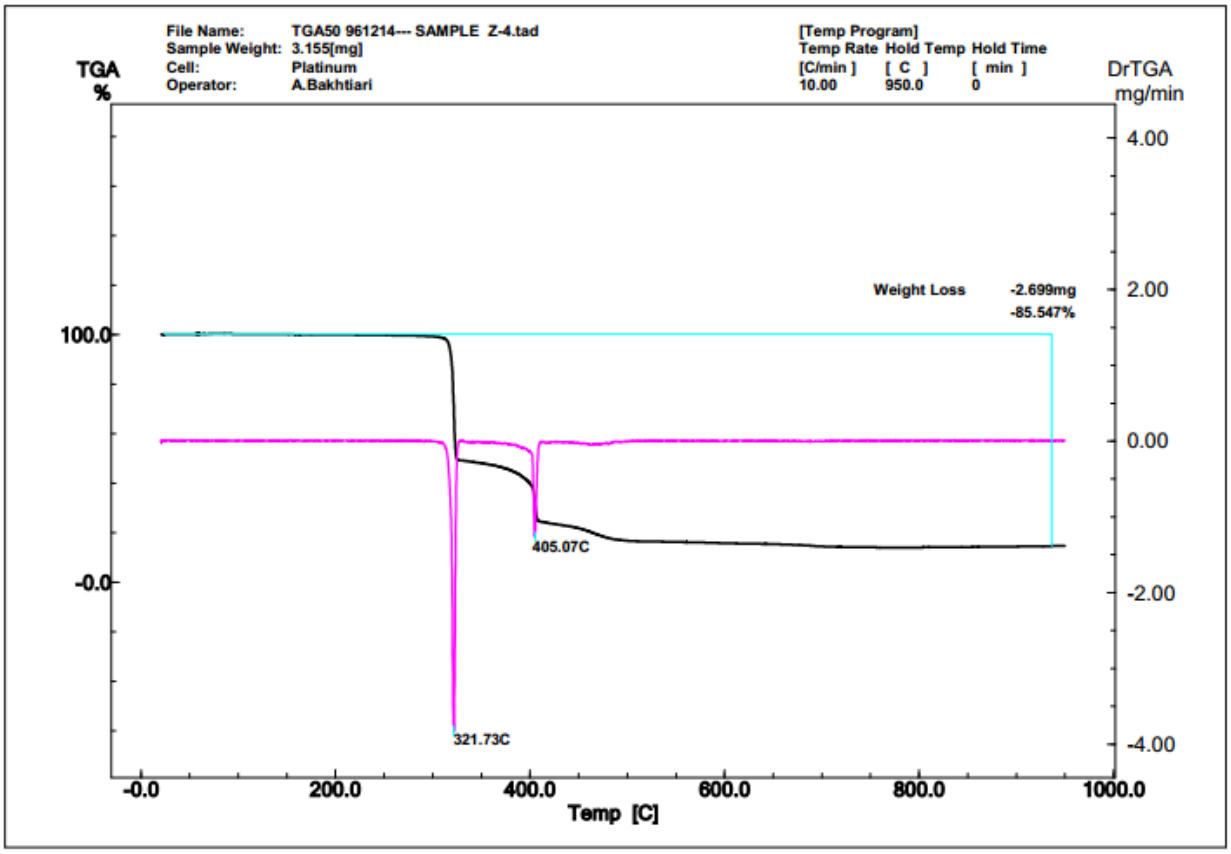


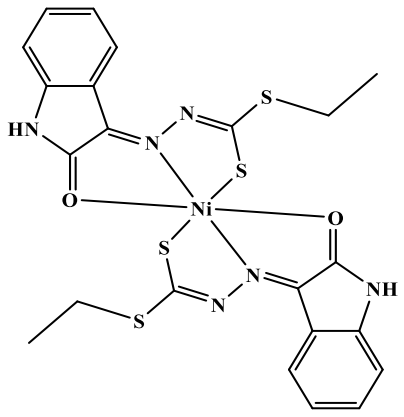


SI 4c. TGA and DTG curves thermogram of **3**.

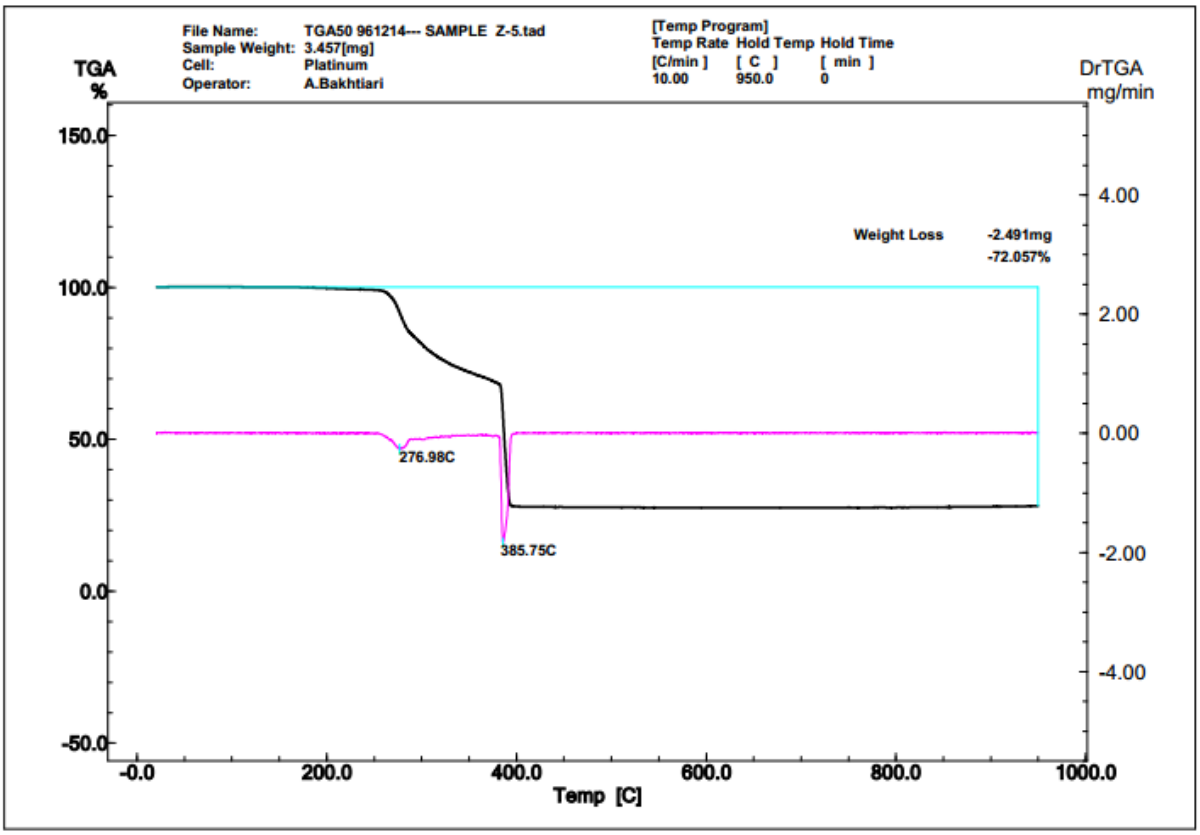


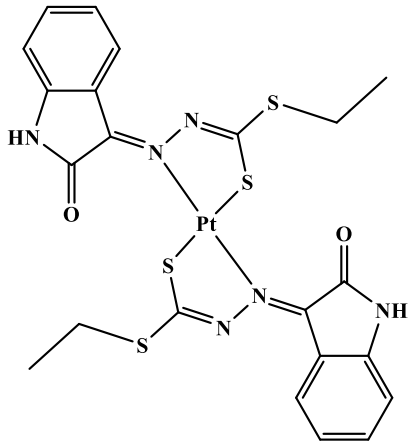


SI 4d. TGA and DTG curves thermogram of **4**.

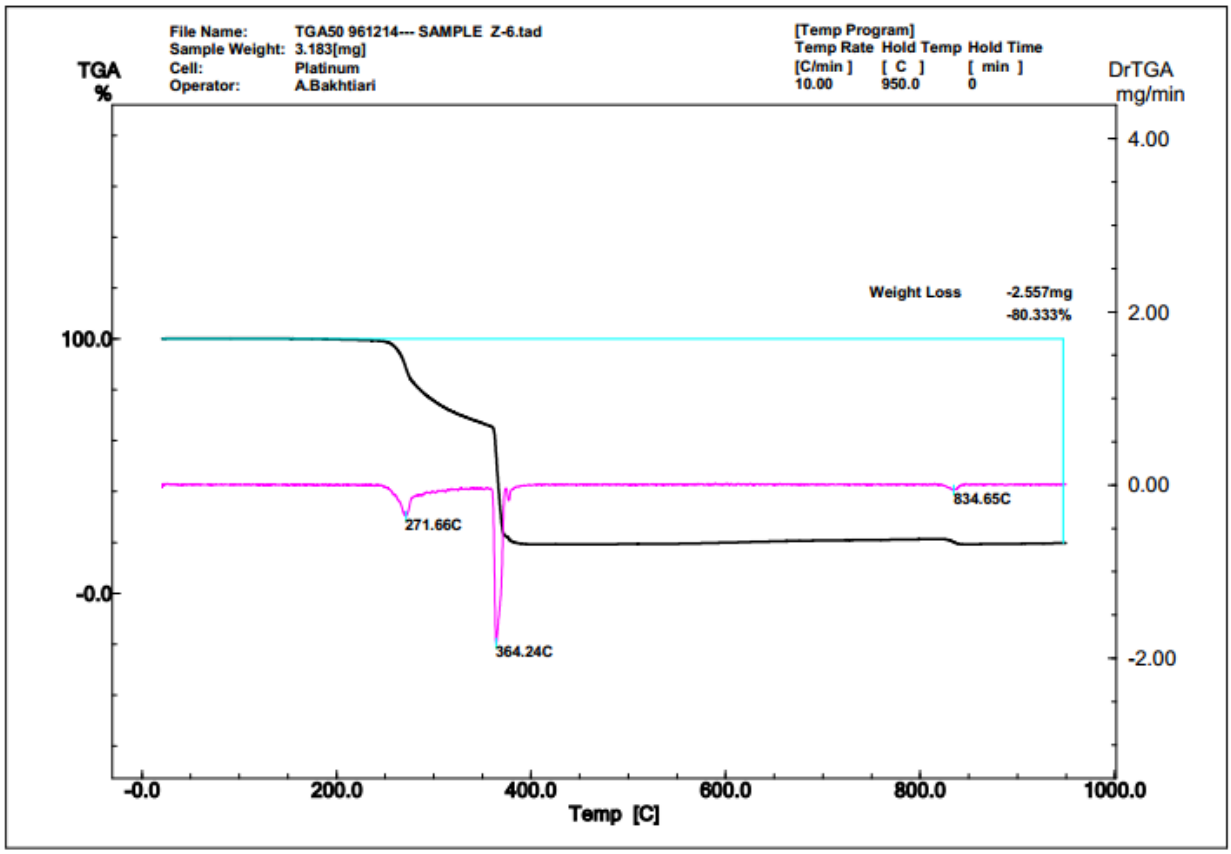


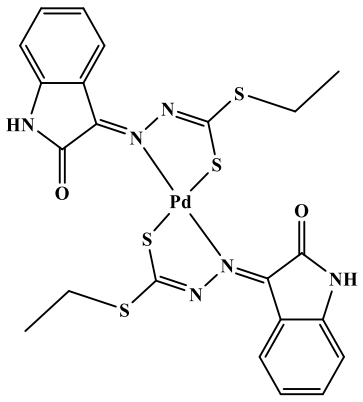


SI 4e. TGA and DTG curves thermogram of **5**.

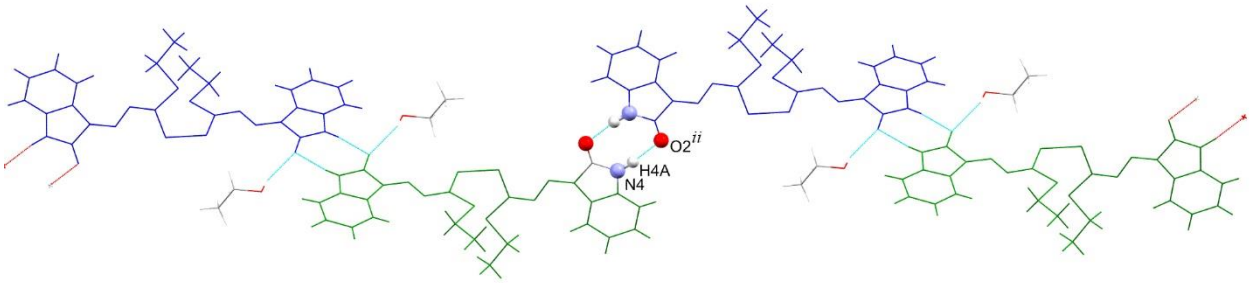


SI 5a. the hydrogen bonds of N4—H4···O2$^{ii}$ (1.895 Å) (symm. code *ii*: -*x*,-*y*,1-*z*) interaction along of [-1 -2 1] vector.

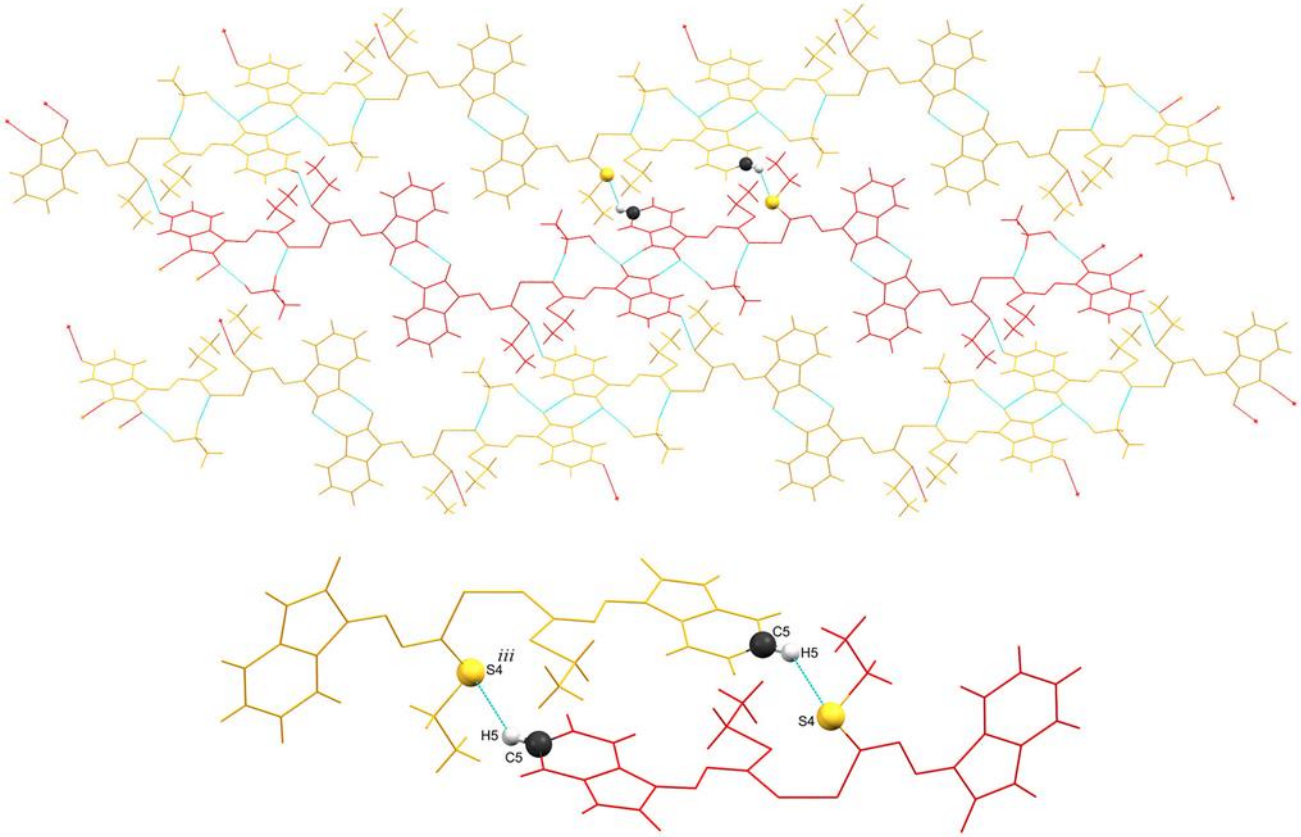


SI 5b. Chains expand through C5—H5···S4$^{iii}$ (2.932 Å) (symm. code *iii*: 2-*x*,1-*y*,-*z*) interaction in direction of [-1 1 0].

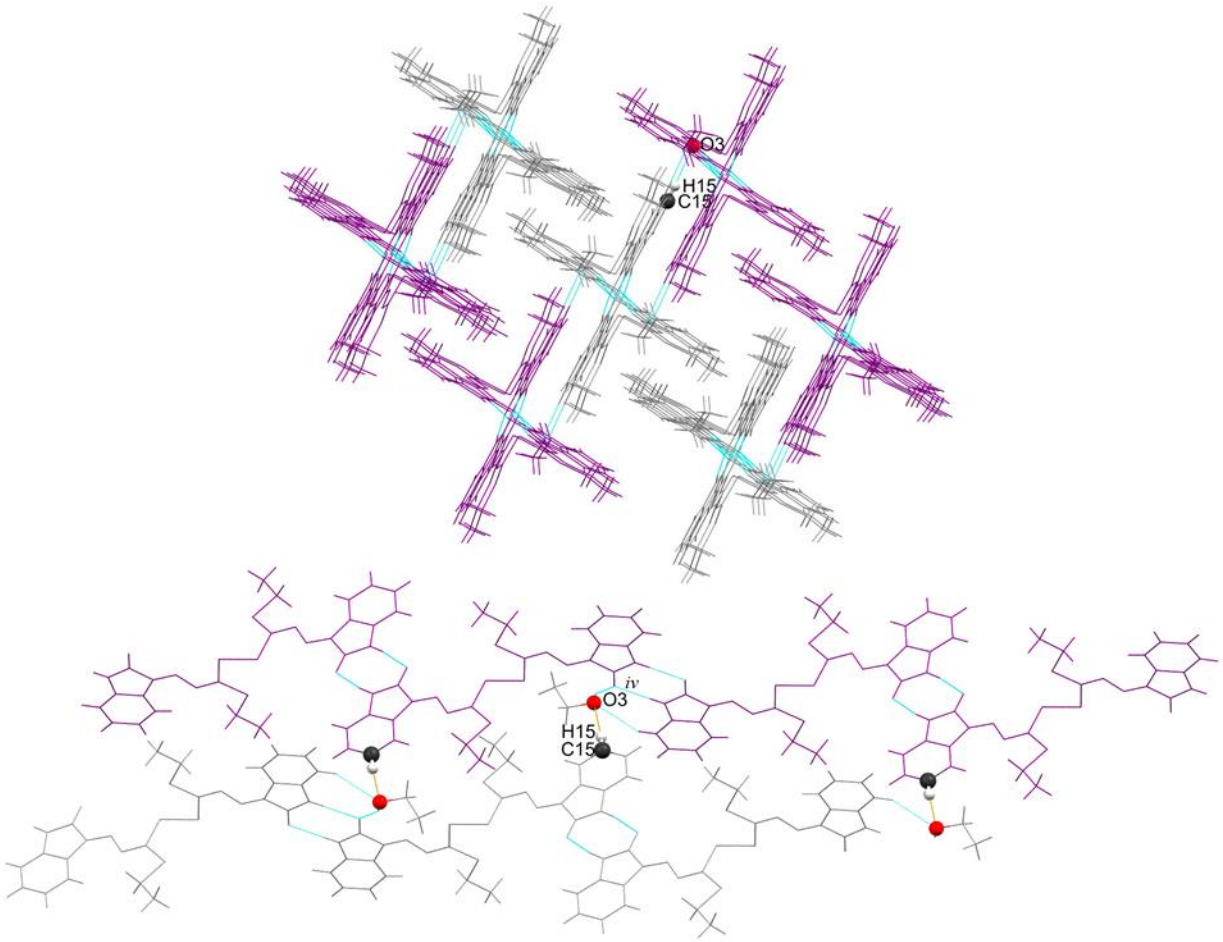


SI 5c. Form of third dimensional through hydrogen bond of C15—H15···O3$^{iv}$ (2.528 Å) (symm. code *iv*: 1+*x*, *y*, *z*).

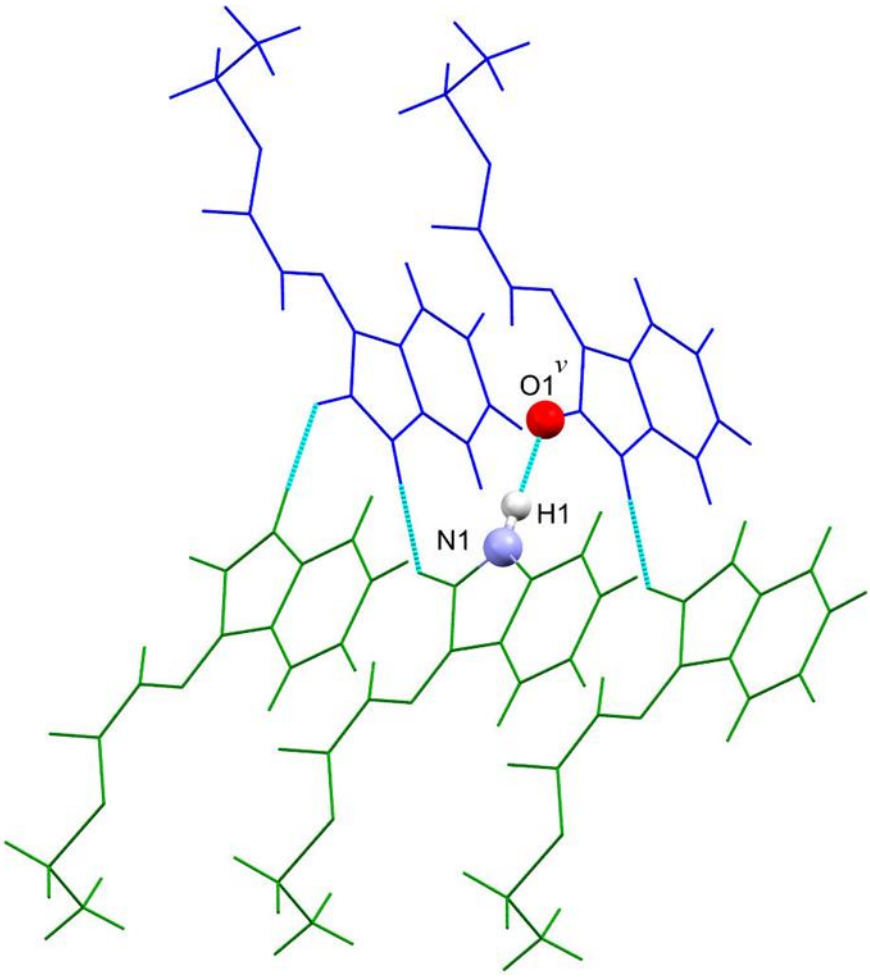


SI 5d. Form a one-dimensional chain in the direction of the *a* axis through the hydrogen bond N1—H1···O1$^{v}$ (2.846 Å) (symm. code *v*: 1/2+x,-1/2-y,1-z).

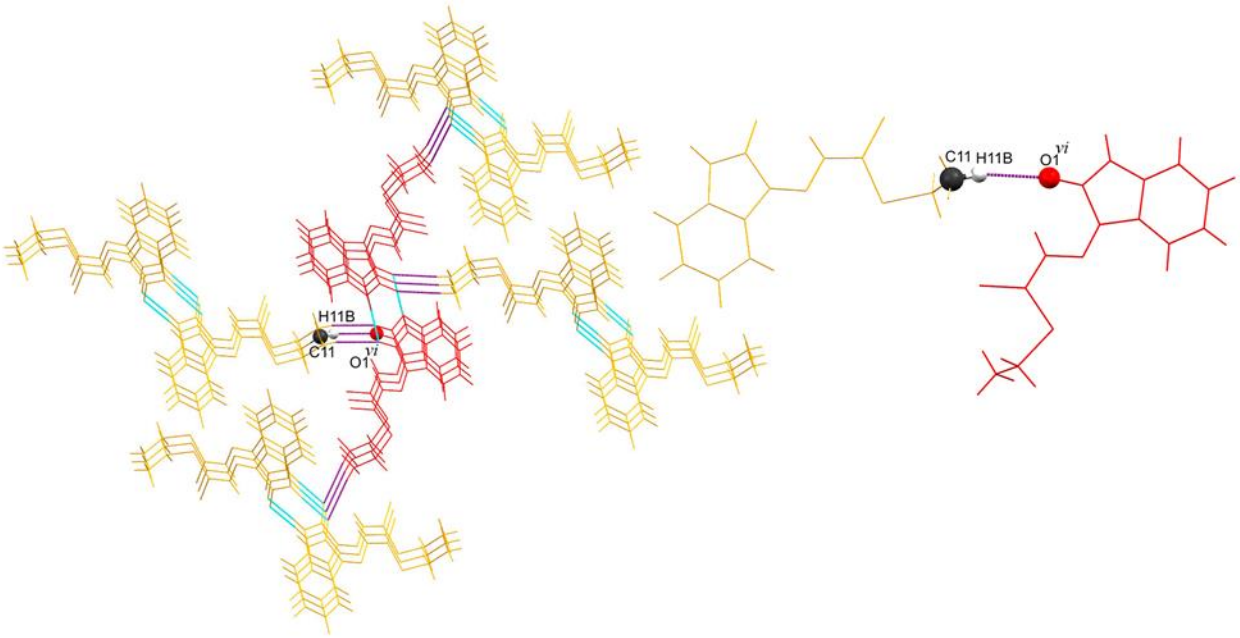


SI 5e. Through C11—H11B···O1$^{vi}$ (3.845 Å) (symm. code *vi*: 1-*x*,1-*y*,1-*z*) hydrogen bonds the second and third dimensions' form along *bc* plane.

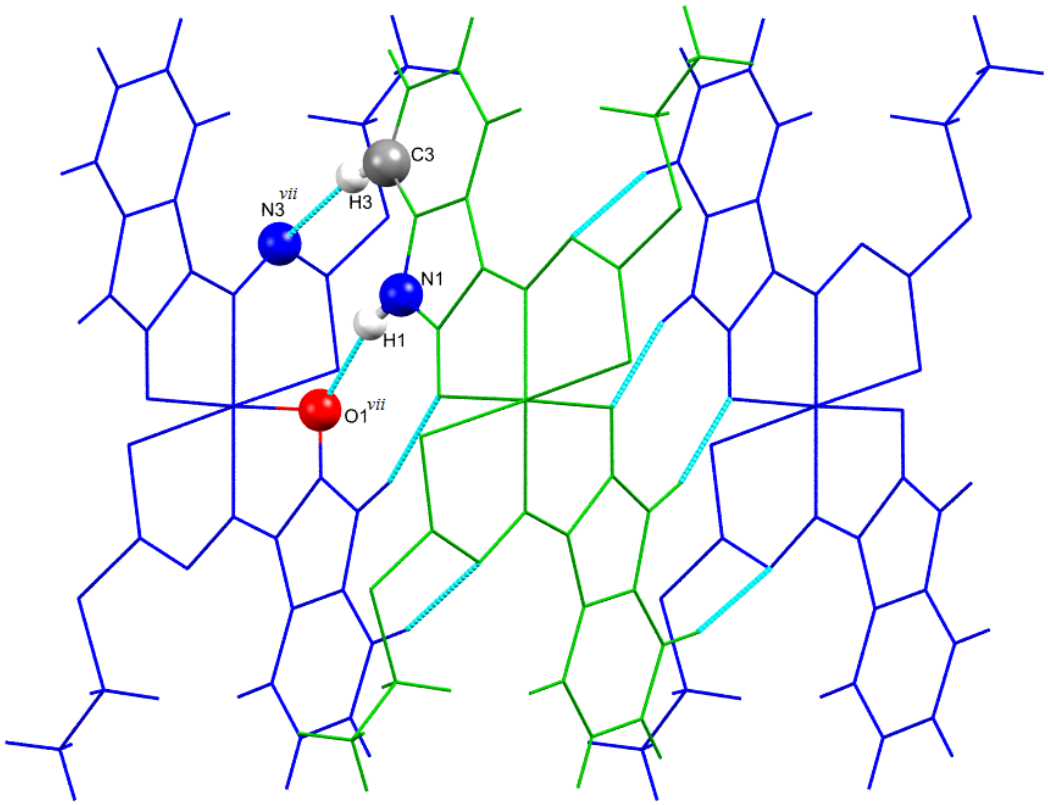


SI 5f. Formation one-dimensional chain for **1** in the direction of the *c* axis through the hydrogen bondings N1—H1···O1$^{vii}$ and C3—H3···N3$^{vii}$ (1.999, and2.636 Å) (symm. code *vii*: *x*,1-*y*,-1/2+*z*).

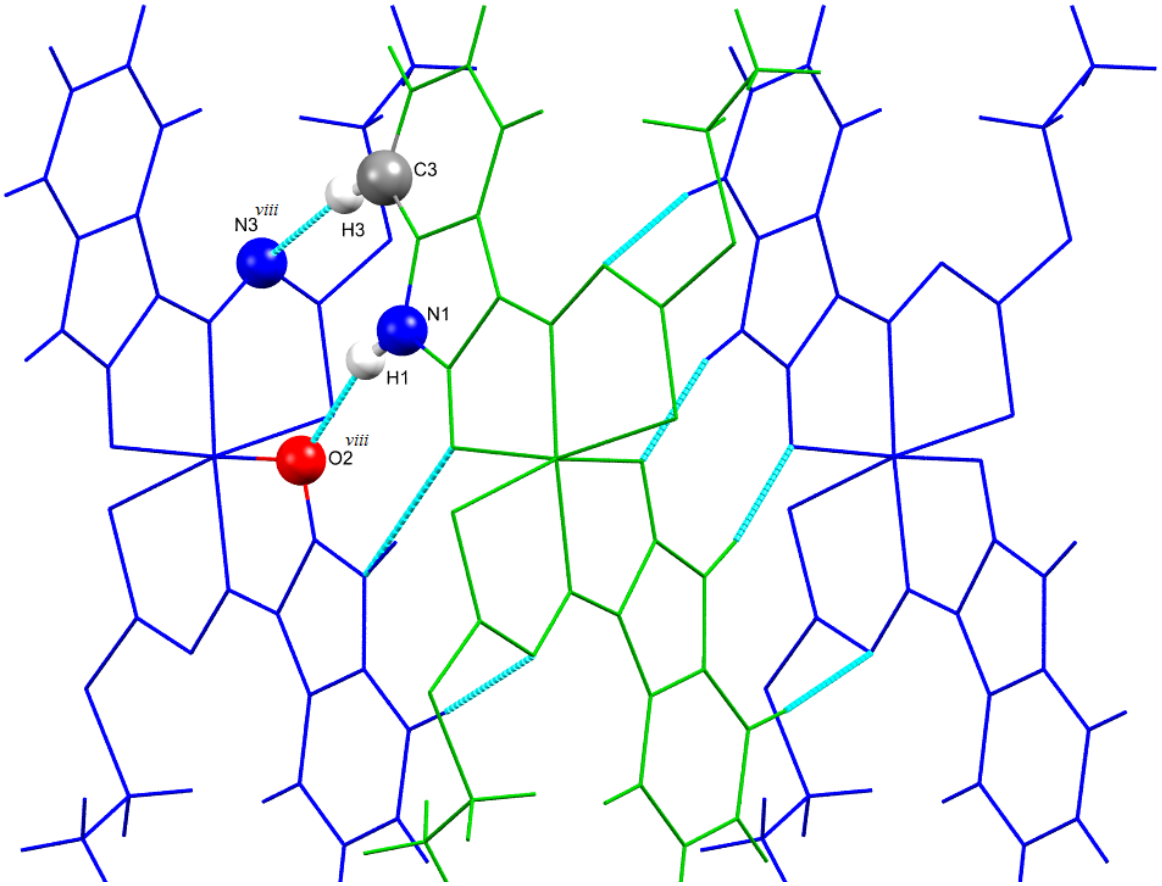


SI 5g. N1—H1···O$^{viii}$ and C3—H3···N3$^{viii}$ (2.009, and2.628 Å) (symm. code *viii*: *x*,1.5-*y*,-1/2+*z*) interaction leads to formation of one-dimensional chain through *c* direction for **2**.

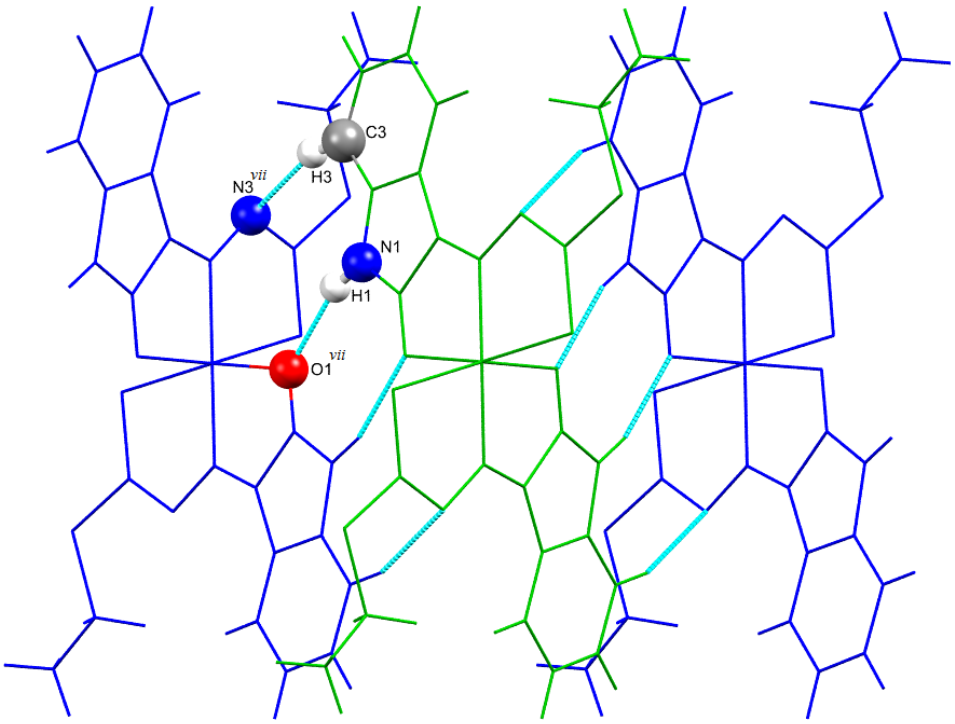


SI 5h. Expanding the chains through N1—H1···O1$^{vii}$ and C3—H3···N3$^{vii}$ (1.999, and 2.004 Å) (symm. code *vii*: *x*,1-*y*, -1/2+*z*) interactions for **3**.

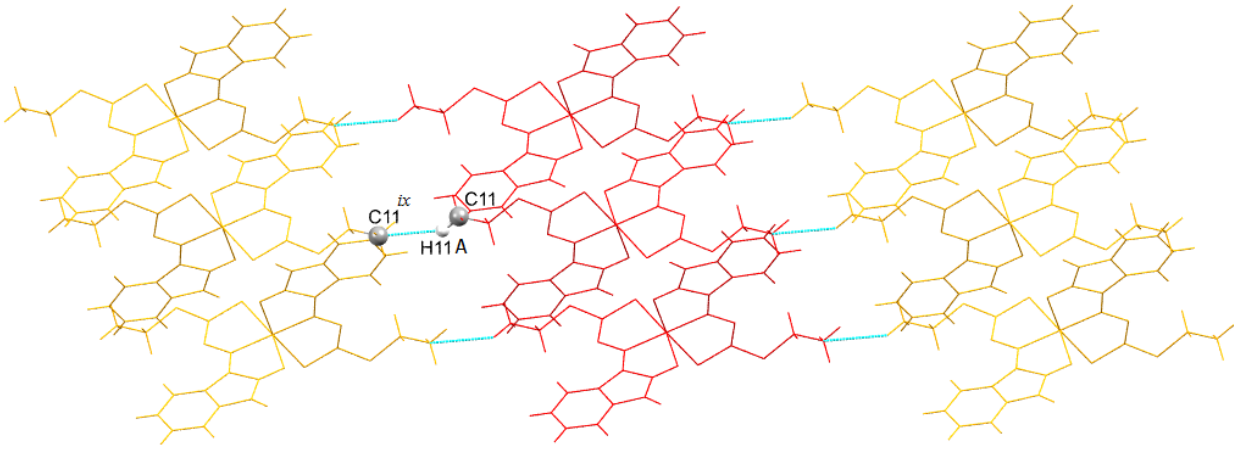


SI 5i. Expanding of the second dimension for **1** along the *ac* plane C11—H11A···C11$^{ix}$ (2.799 Å) (symm. code *ix*: -1+*x*,*y*,*z*) hydrogen bond.

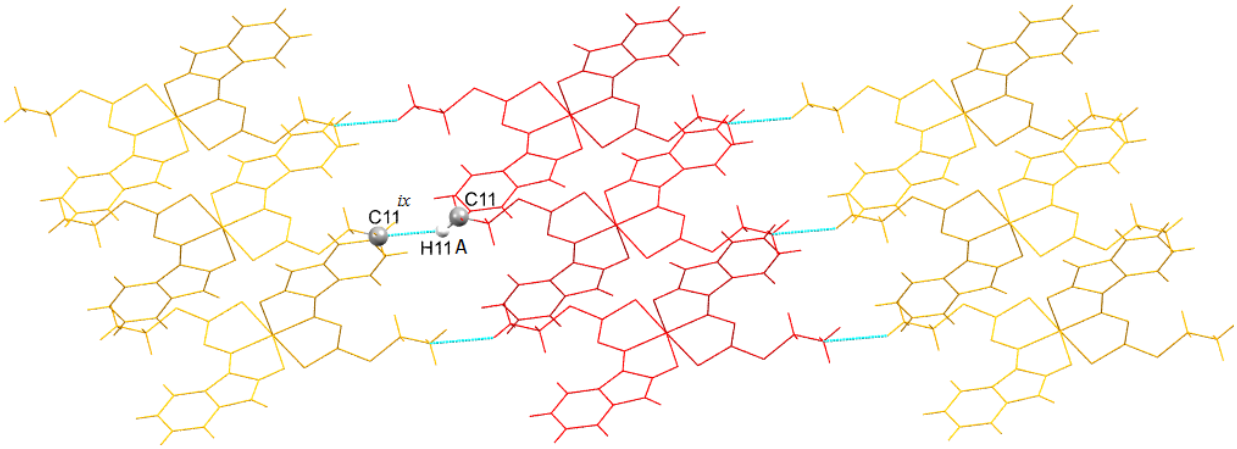


SI 5j. Formation 2D sheets for **2** through C11—H11A···C11$^{ix}$ (2.829 Å) (symm. code *ix*: -1+*x*,*y*,*z*) interactions.

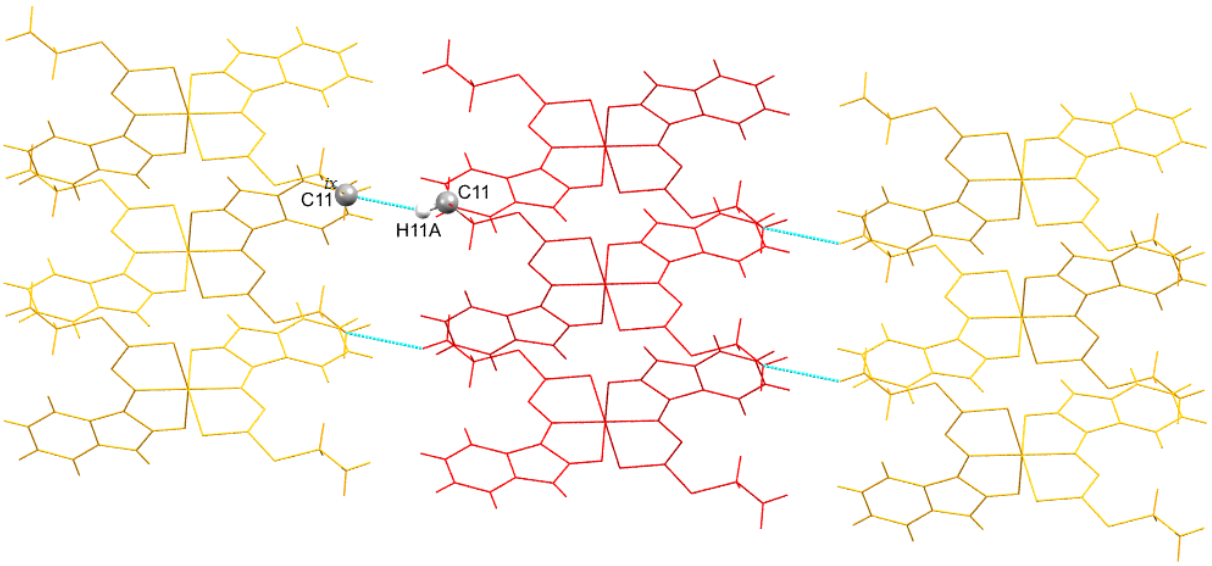


SI 5k. Formation the second dimension for **3** along the *a* axis through the hydrogen bonding of C11—H11A···C11$^{ix}$ (2.927 Å) (symm. code *ix*: -1+*x*,*y*,*z*)

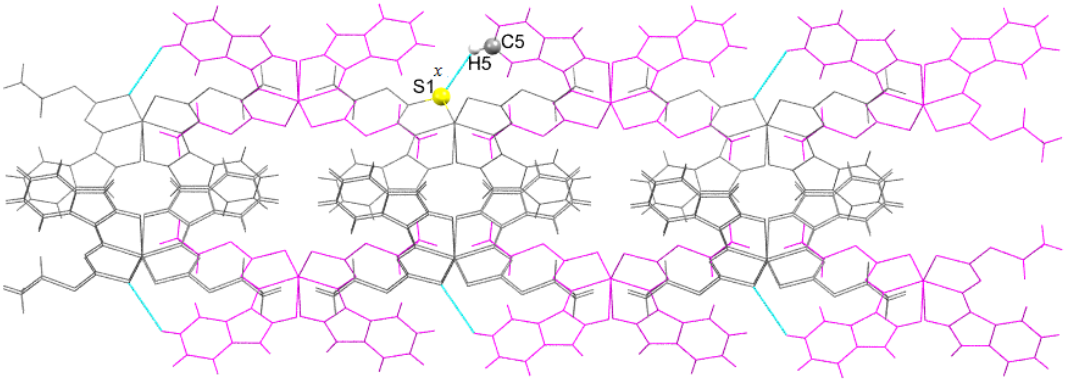


SI 5l. The third dimension for **1** is formed through C5—H5···S1$^{x}$ (3.094 Å) (symm. code *x*: 1-x,*y*,1/2-*z*) interactions along the *b* axis.

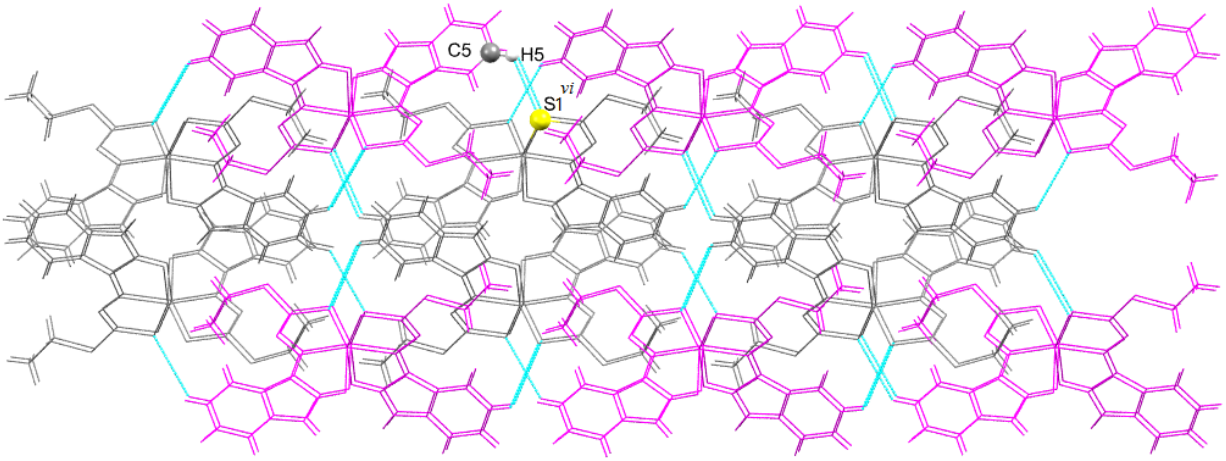


SI 5m. Expanding the planes by C5—H5···S1$^{vi}$ (3.045 Å) (symm. code *vi*: 1-x,1-*y*,1-*z*) interaction to construct the 3D supramolecular network for **2**.

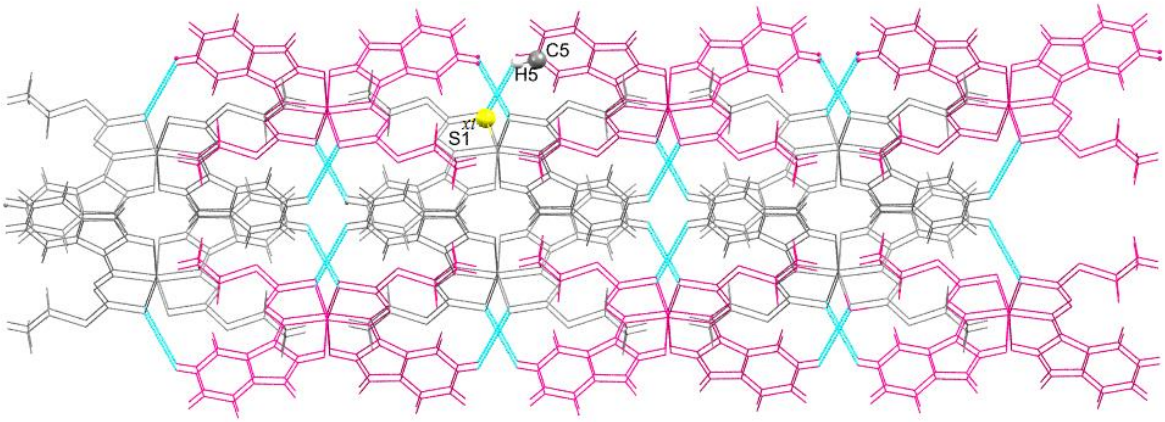


SI 5n. The third dimension for **3** occurs along the *b* axis through C5—H5···S1$^{xi}$ (3.100 Å) (symm. code *xi*: 1-x,*y*,-1/2-*z*) hydrogen bonds.

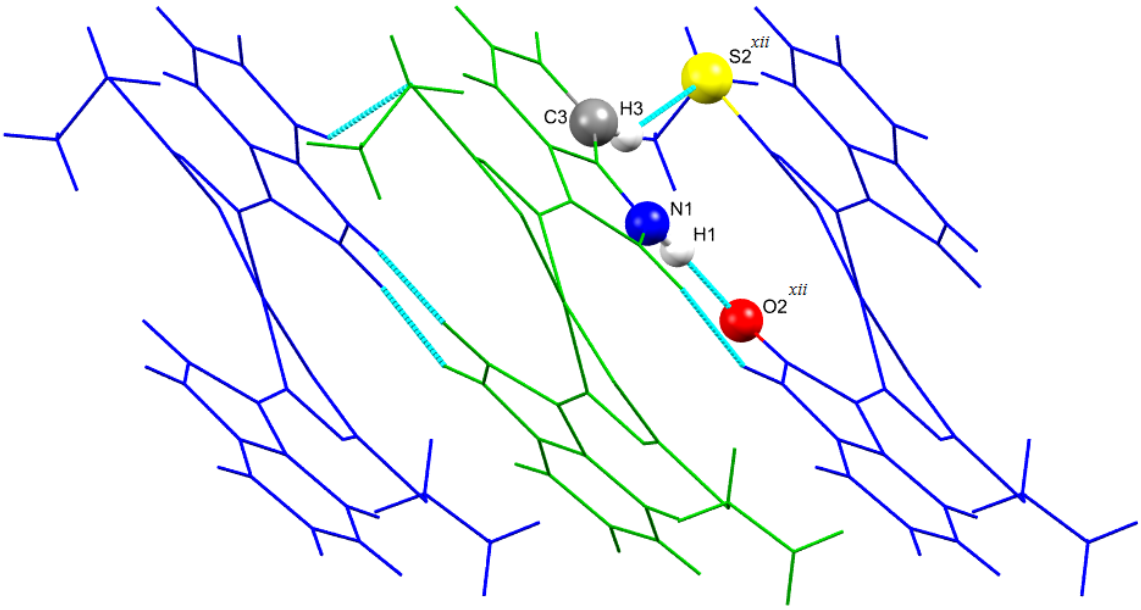


SI 5o. Formation chains along the *b* axis for **4** according to the N1—H1···O1$^{xii}$ (1.930 Å) and C3—H3···S2$^{xii}$ (2.955 Å) (symm. code *xii*: 1/2-*x*,1/2+*y*,1/2+*z*) interactions

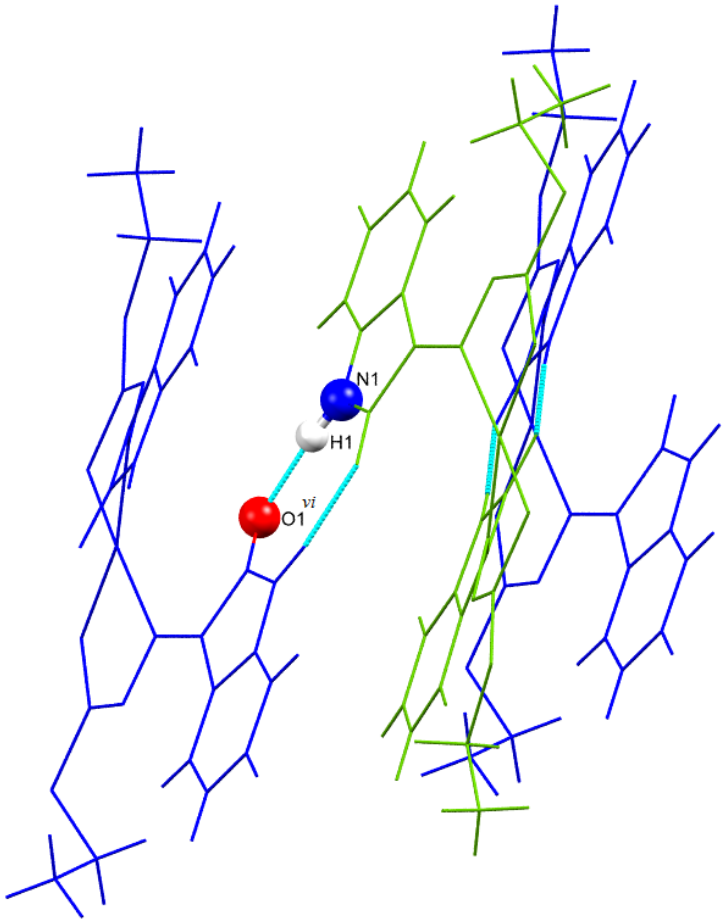


SI 5p. Formation chains along the *c* axis for **5** according to the N1—H1···O1$^{vi}$ (1.986 Å) (symm. code *vi*: 1-*x*,1-*y*,1-*z*) interactions

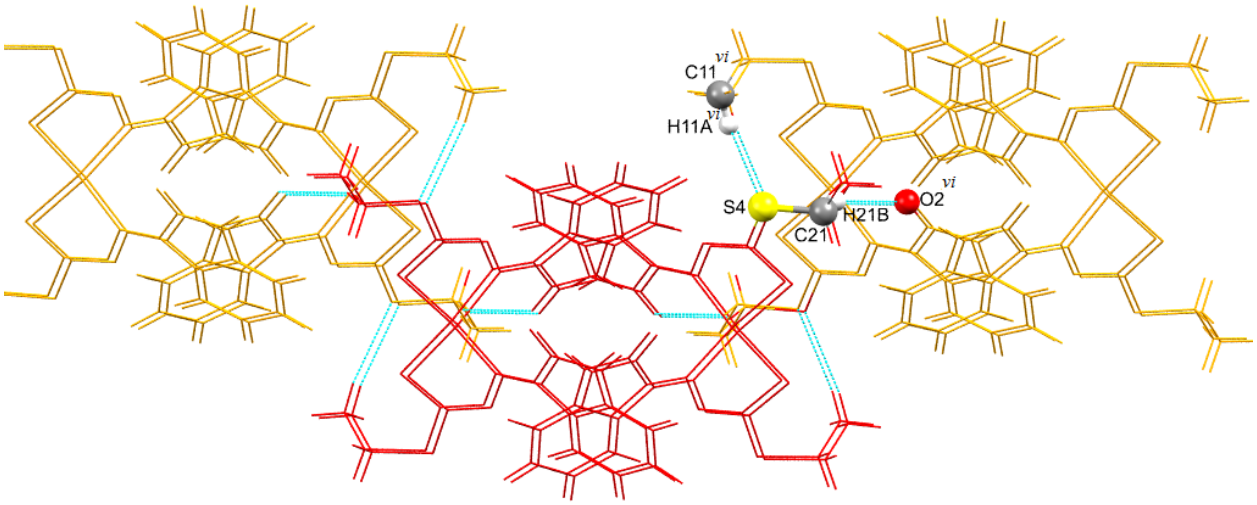


SI 5q. formation the second dimension for **4** through hydrogen bonds of C21—H21B···O2$^{vi}$ (2.600 Å) and C11—H11A···S4$^{vi}$ (2.976 Å) (symm. code *vi*: 1-*x*,1-*y*,1-*z*).

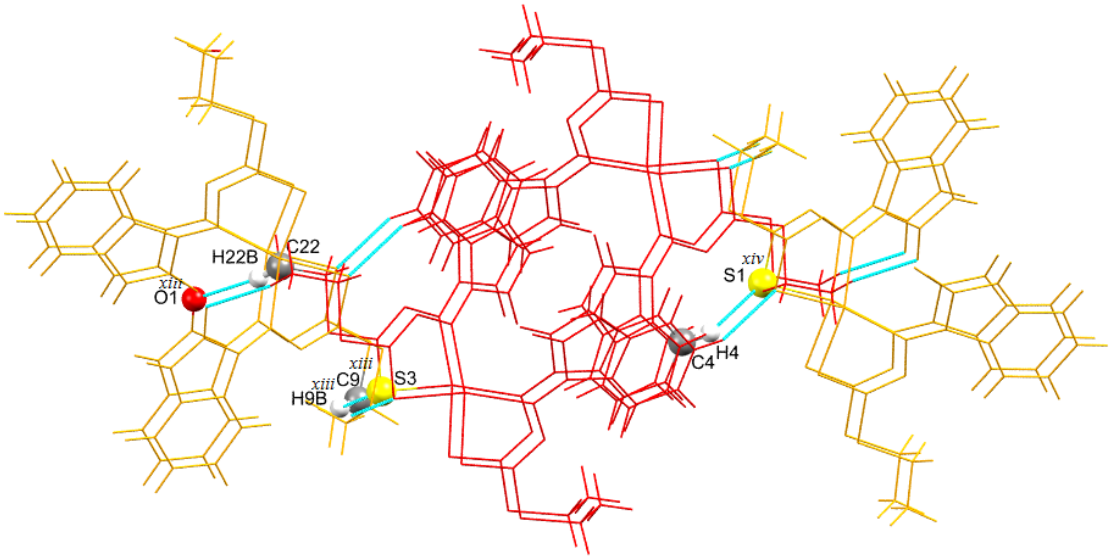


SI 5r. formation the second dimension for **5** through hydrogen bonds of C22—H22B···O1$^{xiii}$ (2.478 Å), C9—H9B···S3$^{xiii}$ (2.966 Å), C4—H4···S1$^{xiv}$ (2.762 Å) (symm. code *xiii*: *x*,1/2-*y*,1/2+*z*, *xiv:* 1-*x*,1/2+*y*,1/2-*z*)

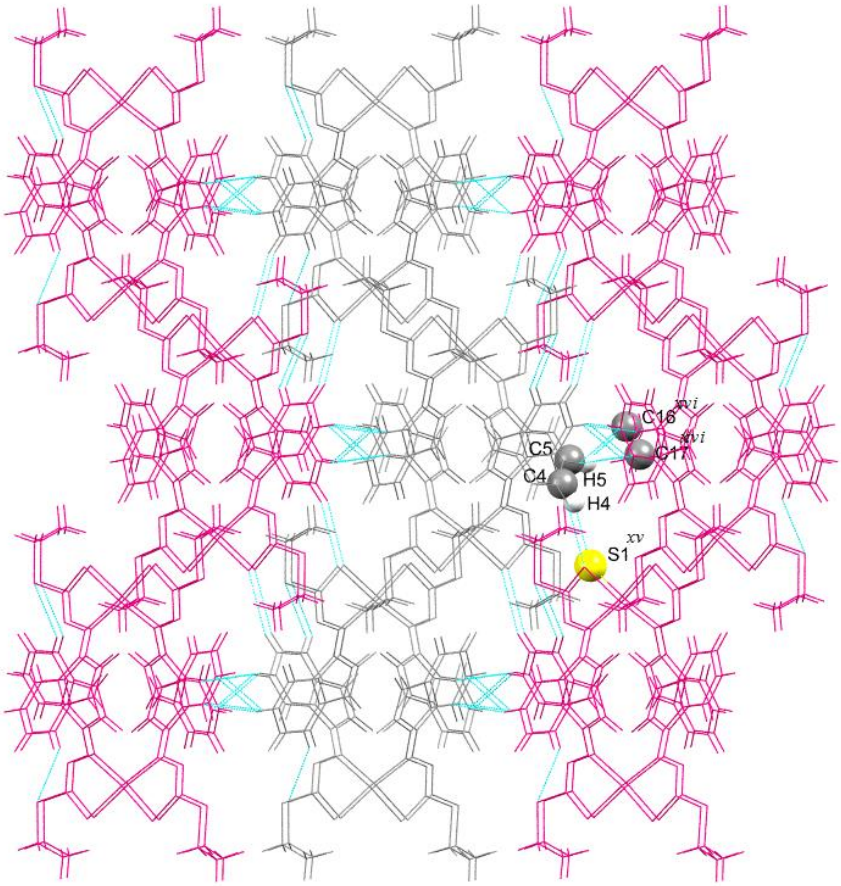


SI 5s. Expanding of the third dimension for **4** *via* C4—H4···S1$^{xv}$ (2.926 Å) and C5—H5···C16/17$^{xvi}$ (2.787/2.701 Å) (symm. Code *xv*: 1/2+*x*, *y*,1.5-*z*, *xvi*: 1.5-*x*,1-*y*,1/2+*z*) interaction.

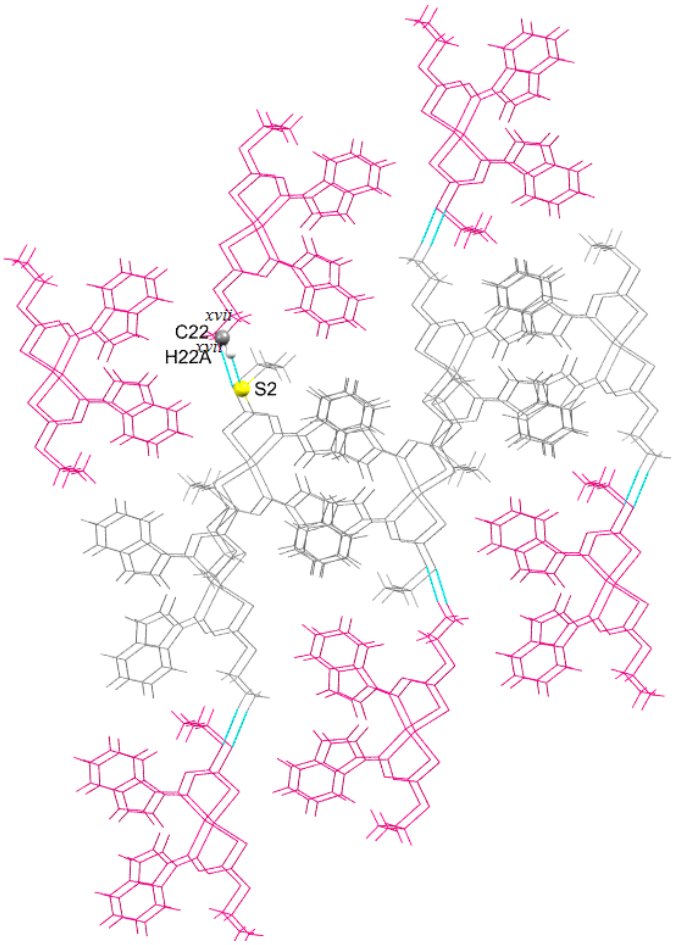


SI 5t. Expanding of the third dimension for **5** along *c* axis *via* C22—H22A···S2$^{xvii}$ (2.743 Å) (symm. code *xvii*: -1+*x*,*y*,-1+*z*) interaction.

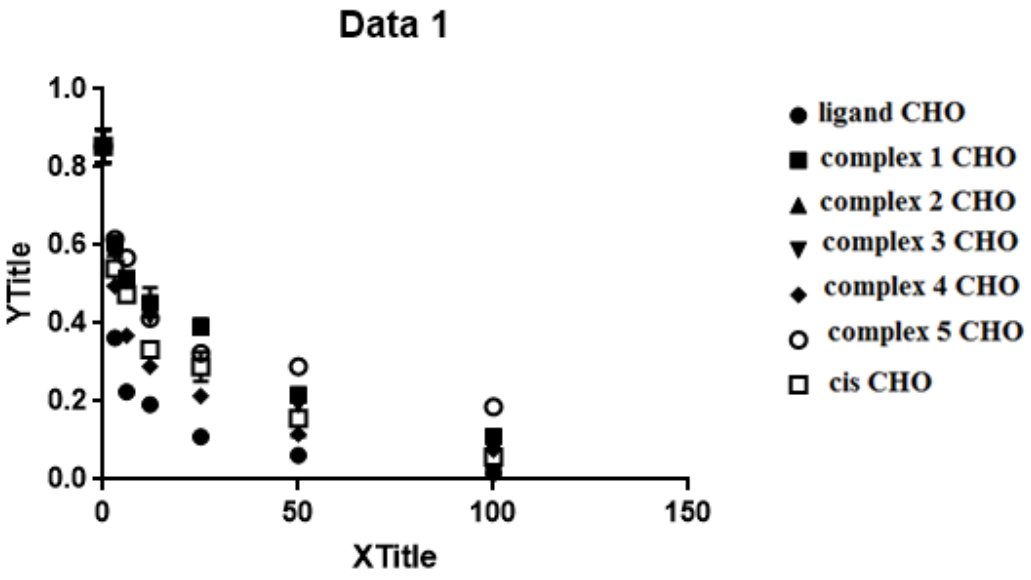


SI 6a. Graph of cytotoxicity test against normal cell of CHO.

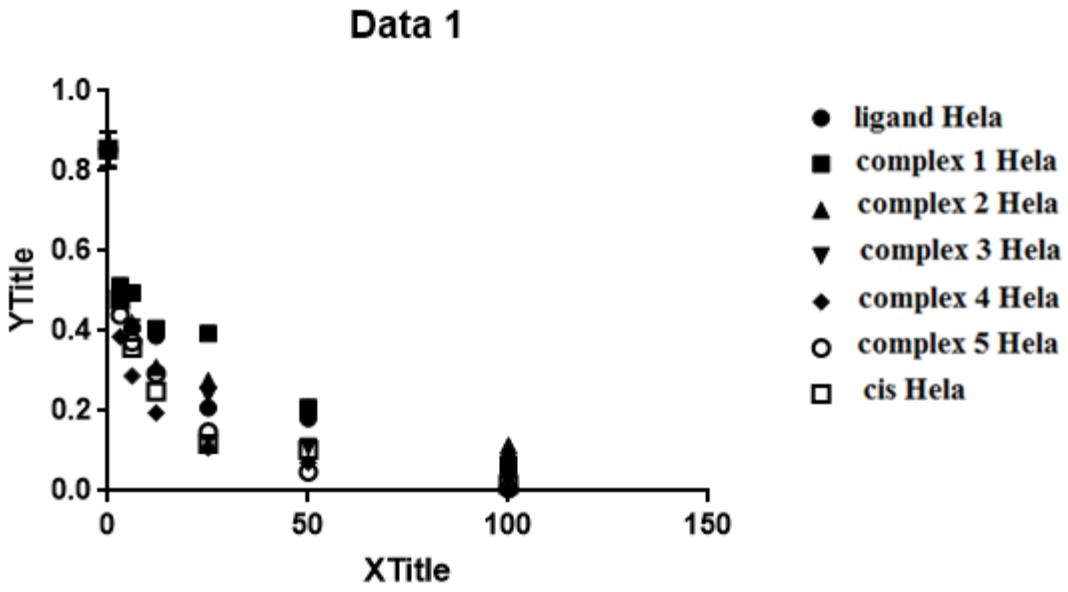


SI 6b. Graph of cytotoxicity test against cancer cell of Hela.

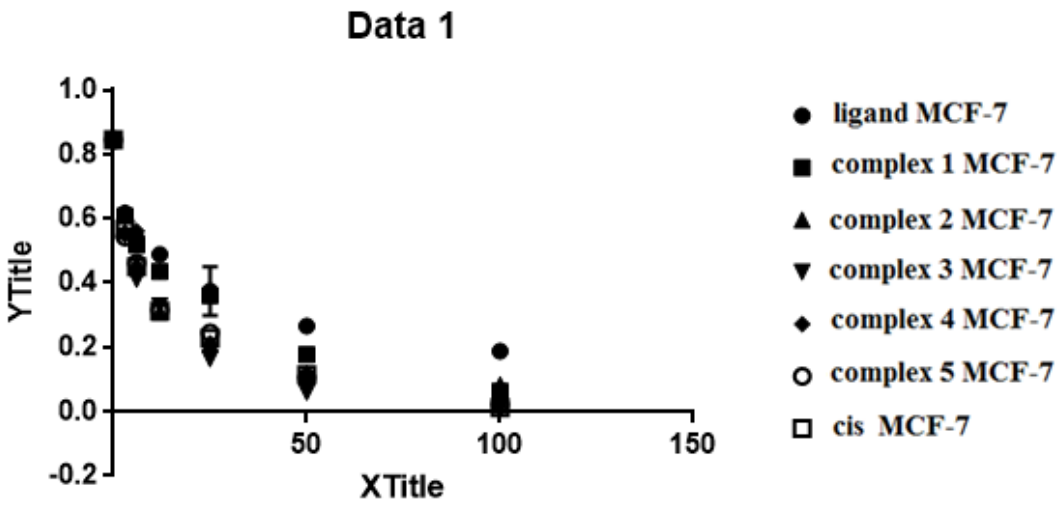


SI 6c. Graph of cytotoxicity test against cancer cell of MCF-7.

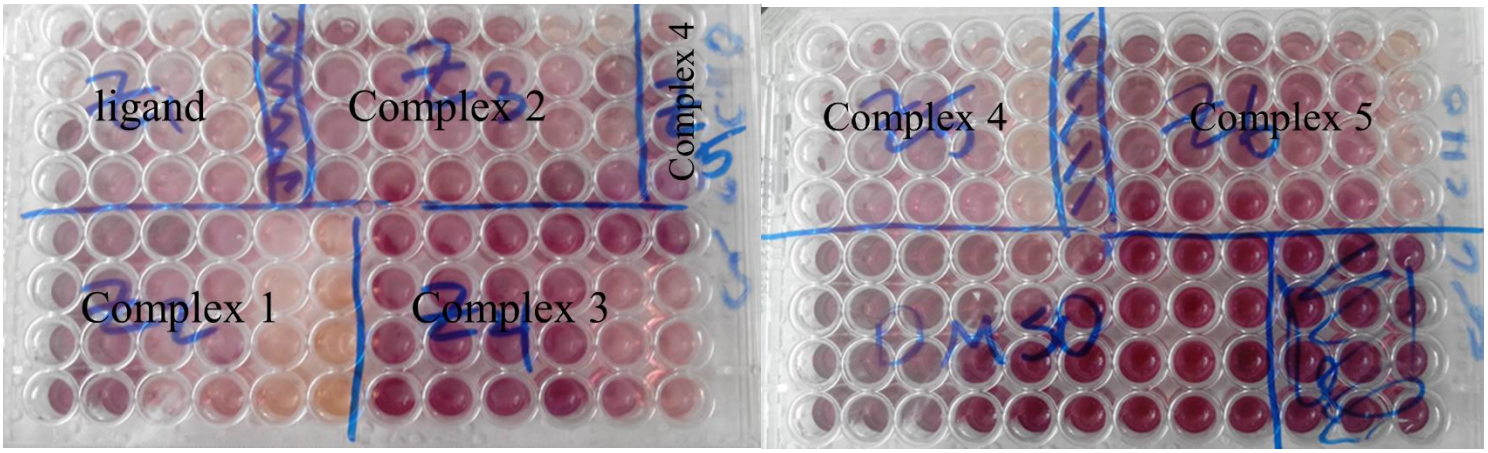


SI 6d. The pictures of the color change of compounds during the MTT experiment against normal cell of CHO.

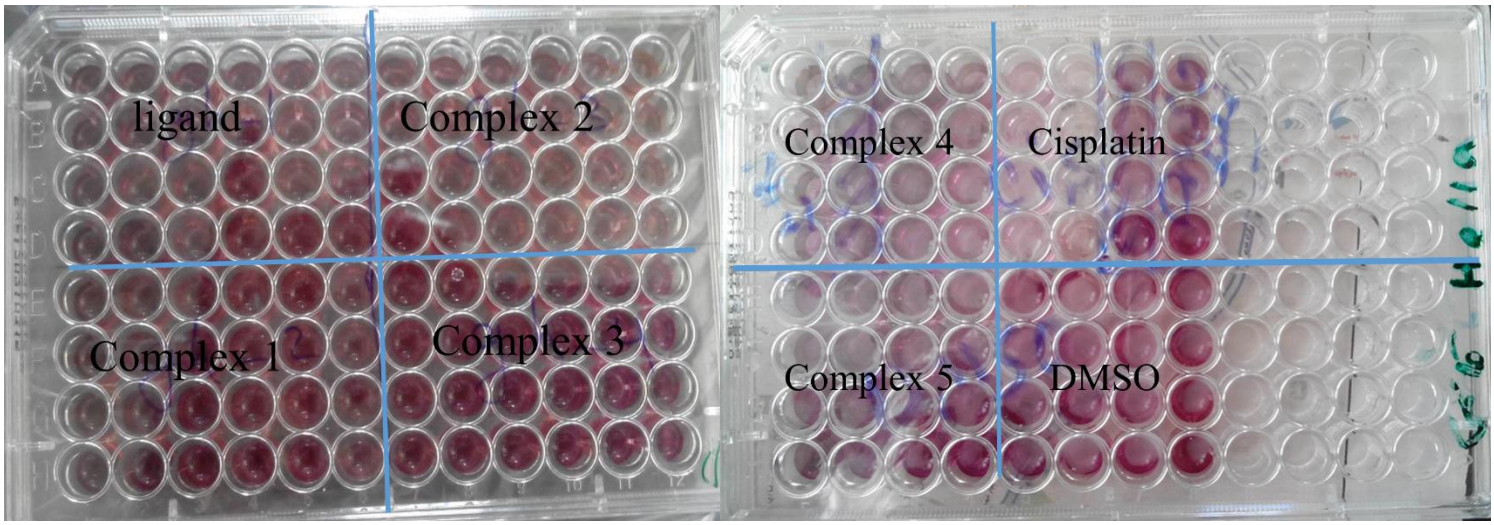


SI 6e. The pictures of the color change of compounds during the MTT experiment against cancer cell of Hela.

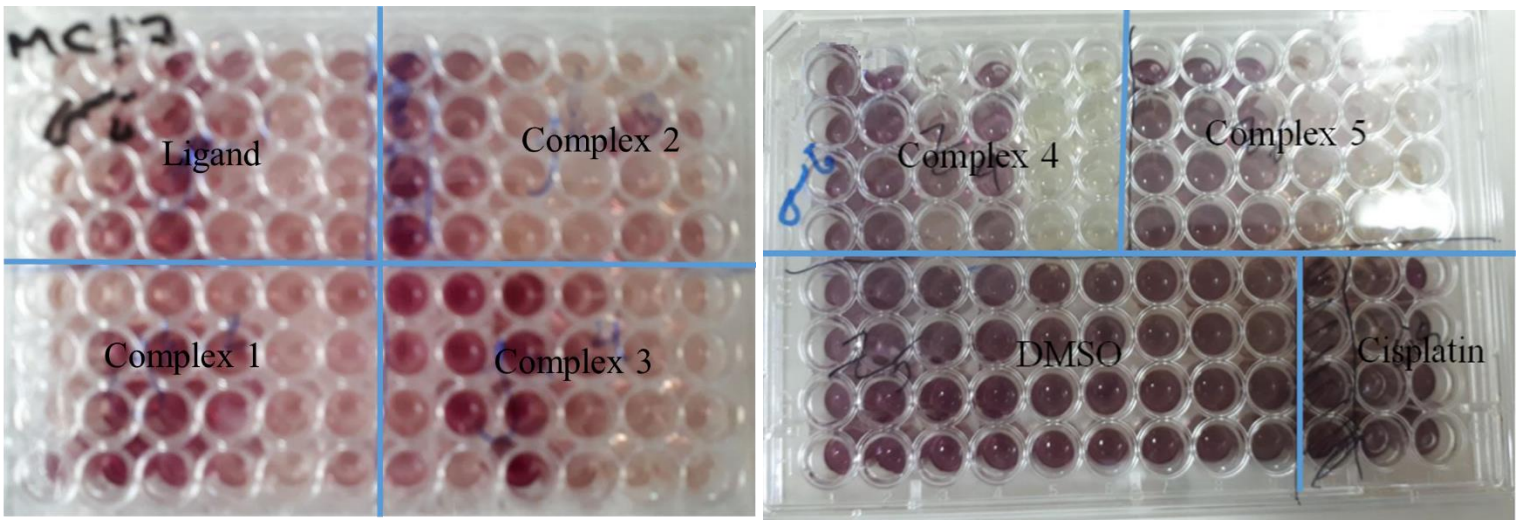


SI 6f. The pictures of the color change of compounds during the MTT experiment against cancer cell of MCF-7.

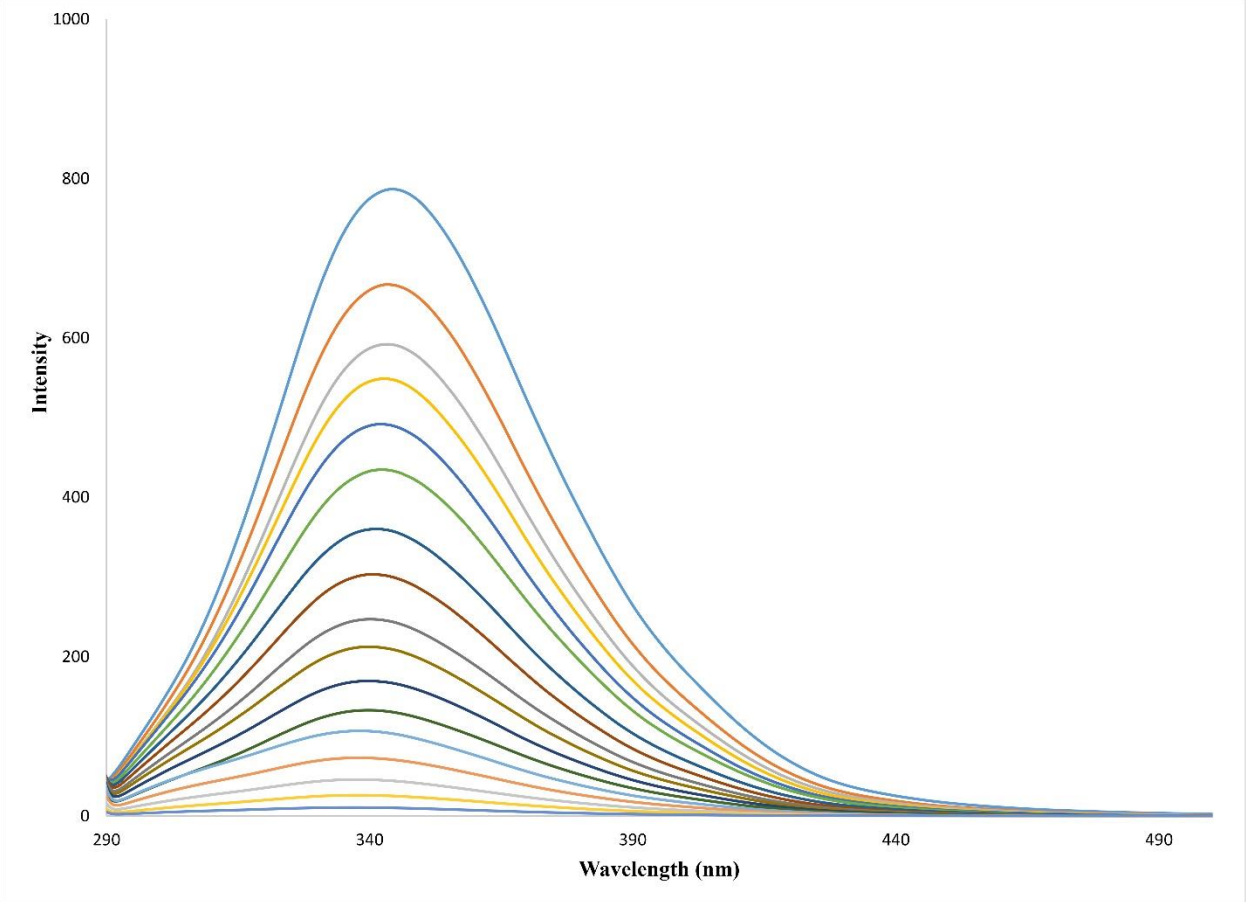


SI 7a. Fluorescence quenching spectra of HSA in the presence of increasing concentration of **1**. [HSA] = 15 μM, [**1**] = 0-16 μM, $\lambda_{ex}$ = 280 nm, T = 298 K.

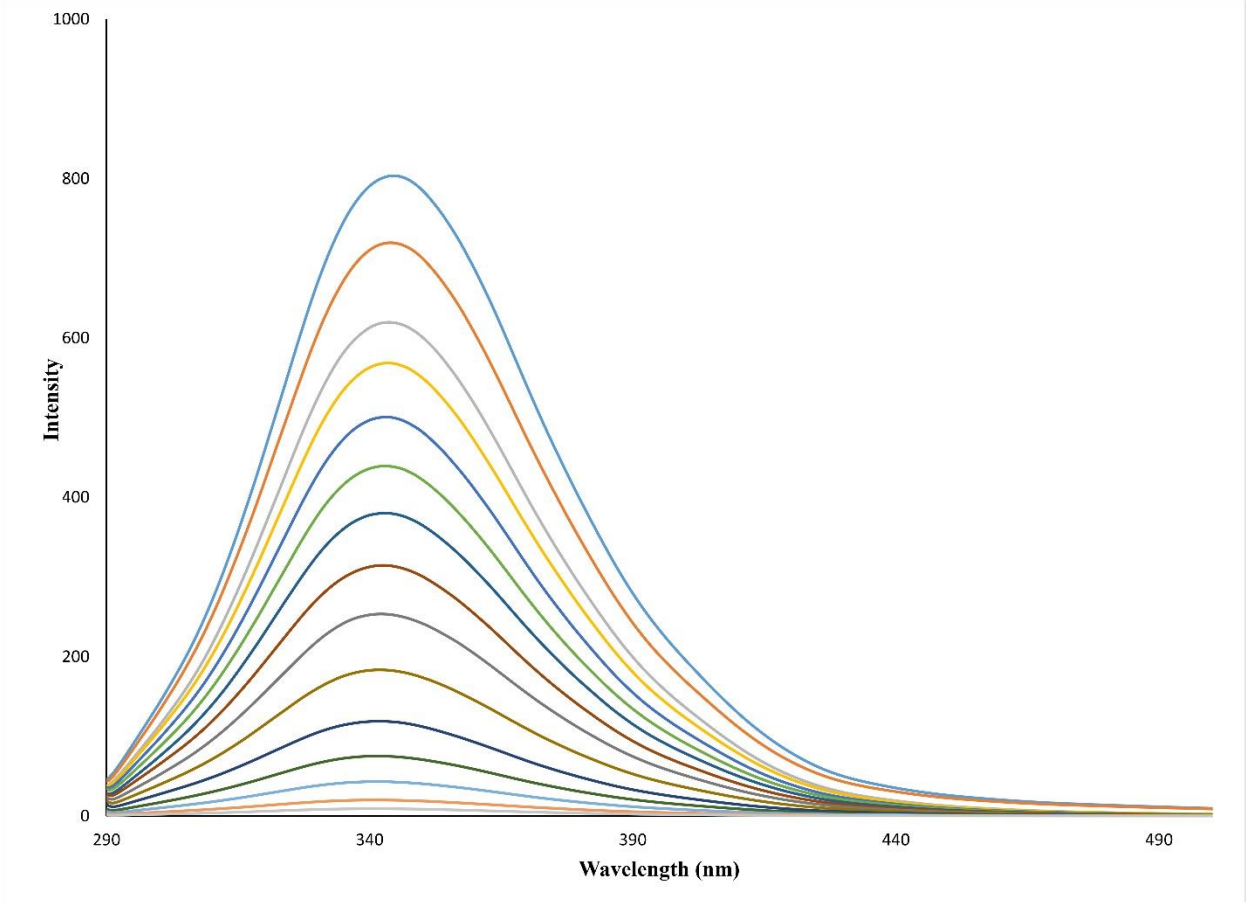


SI 7b. Fluorescence quenching spectra of HSA in the presence of increasing concentration of **2**. [HSA] = 15 μM, [**2**] = 0-16 μM, $\lambda_{ex}$ = 280 nm, T = 298 K.

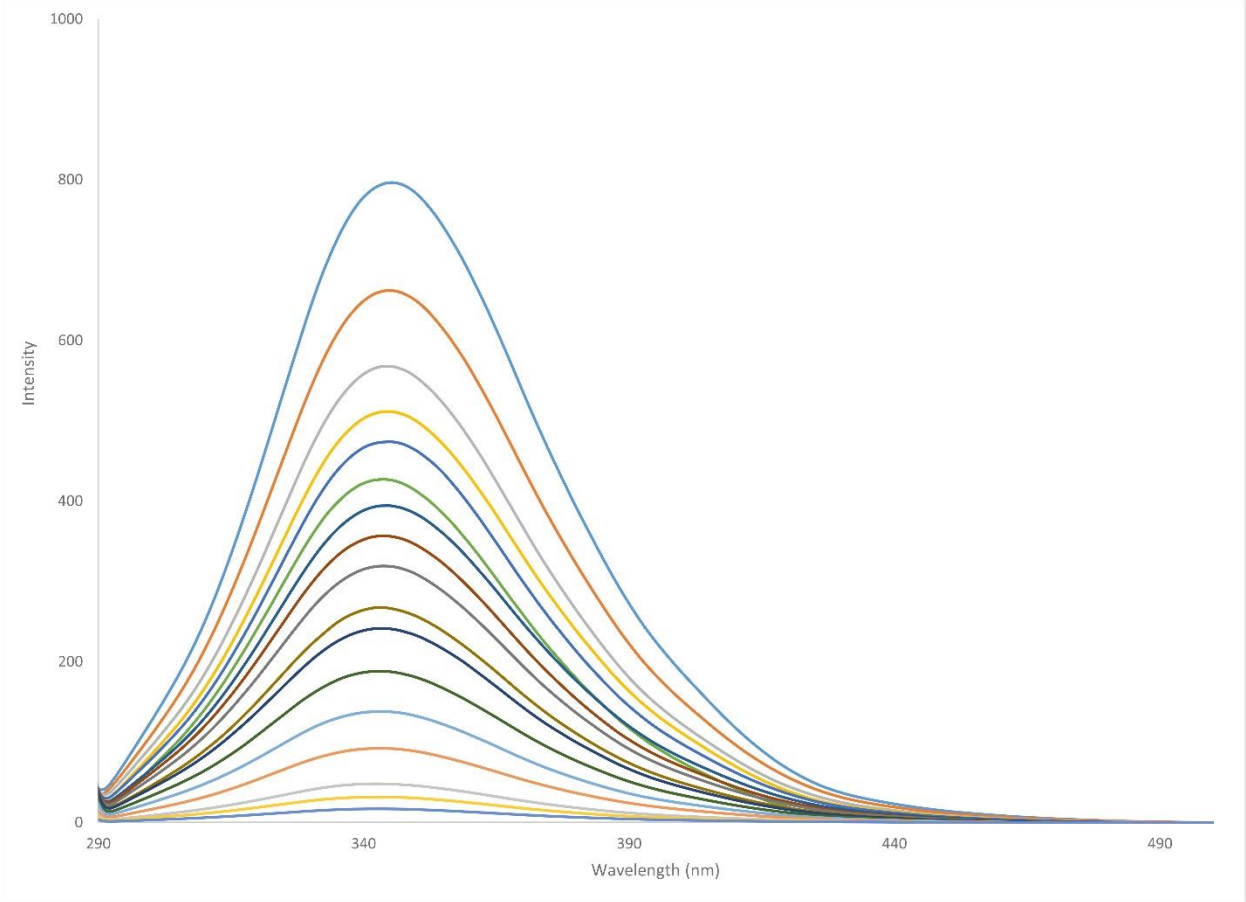


SI 7c. Fluorescence quenching spectra of HSA in the presence of increasing concentration of **3**. [HSA] = 15 μM, [**3**] = 0-16 μM, $\lambda_{ex}$ = 280 nm, T = 298 K.

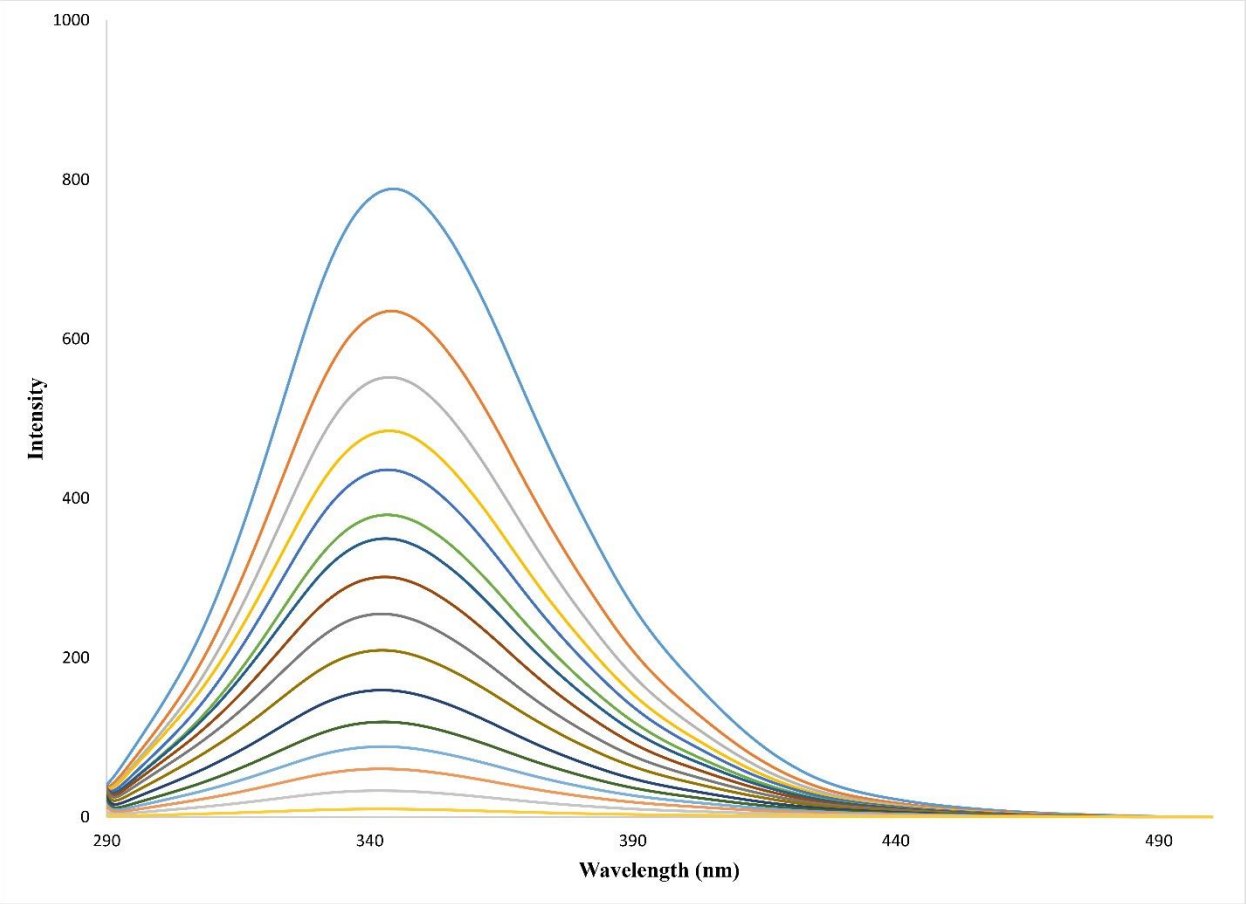


SI 7d. Fluorescence quenching spectra of HSA in the presence of increasing concentration of **4**. [HSA] = 15 μM, [**4**] = 0-16 μM, $\lambda_{ex}$ = 280 nm, T = 298 K.

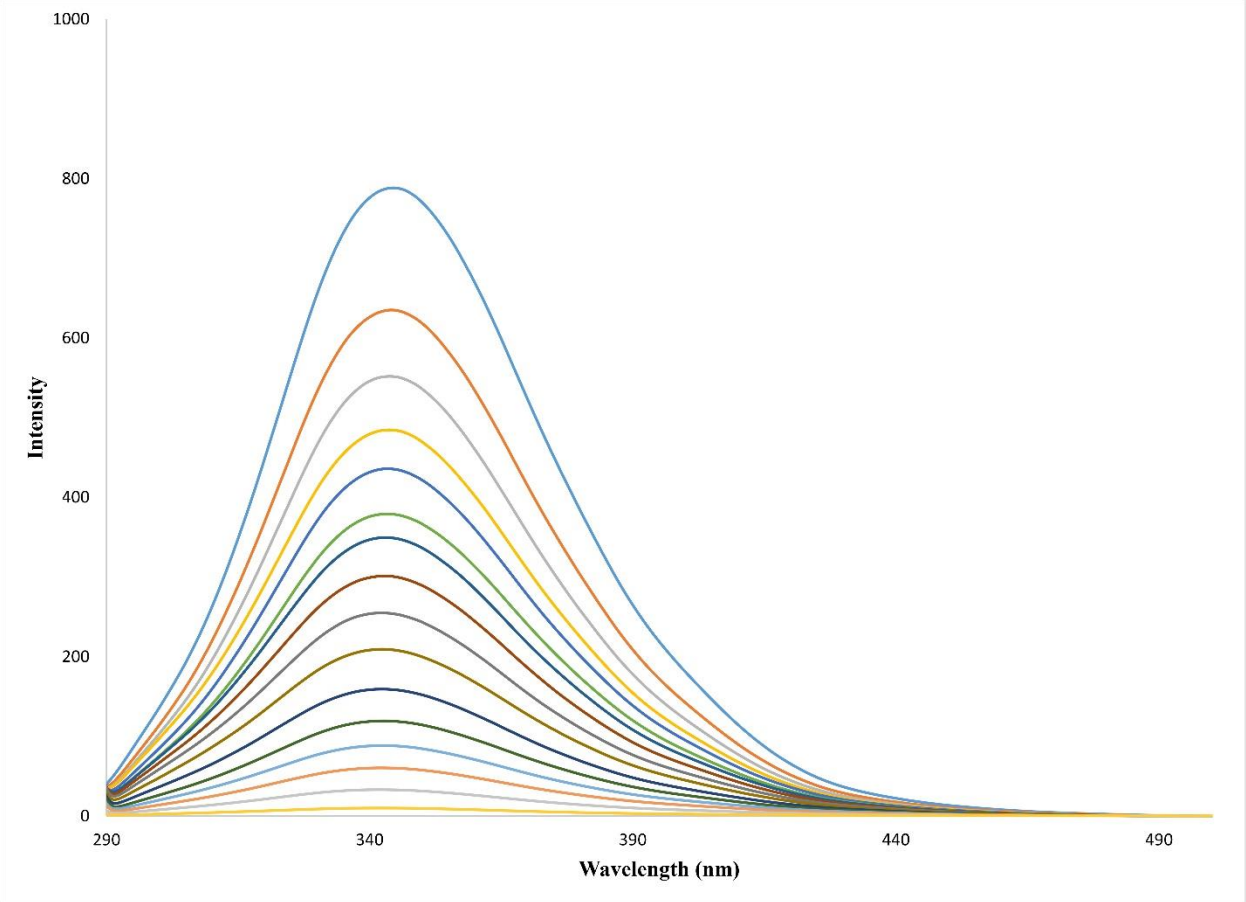


SI 7e. Fluorescence quenching spectra of HSA in the presence of increasing concentration of **5**. [HSA] = 15 μM, [**5**] = 0-16 μM, $\lambda_{ex}$ = 280 nm, T = 298 K.

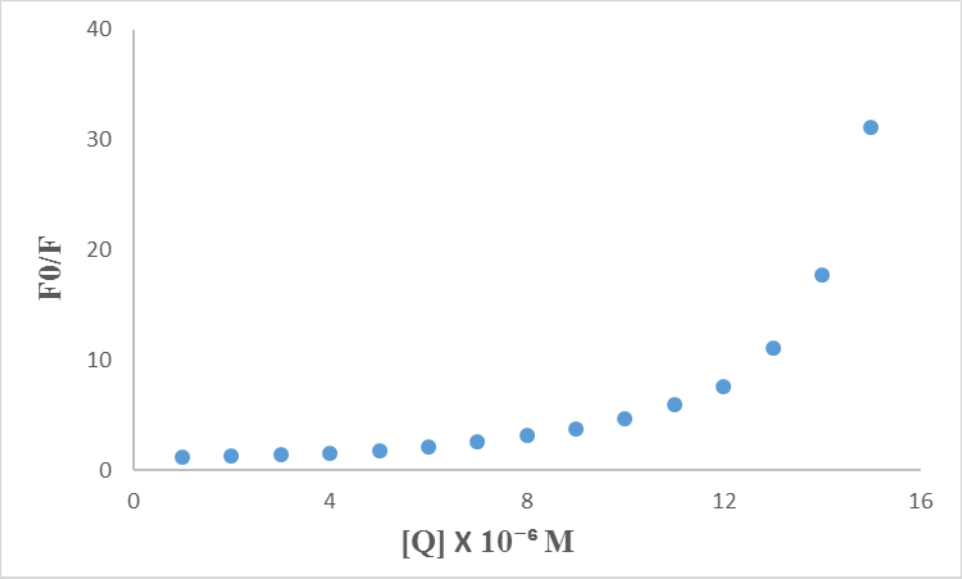


SI 7f. Stern-Volmer plot for quenching of HSA (15 μM) fluorescence by **1** at different concentrations ($\lambda_{ex}$ = 280 nm, $\lambda_{em}$ = 344 nm).

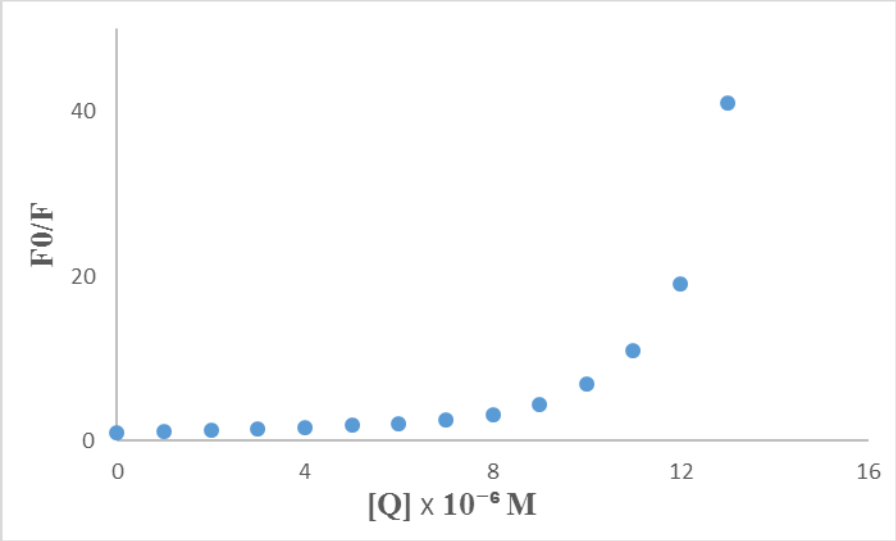


SI 7g. Stern-Volmer plot for quenching of HSA (15 μM) fluorescence by **2** at different concentrations ($\lambda_{ex}$ = 280 nm, $\lambda_{em}$ = 347 nm).

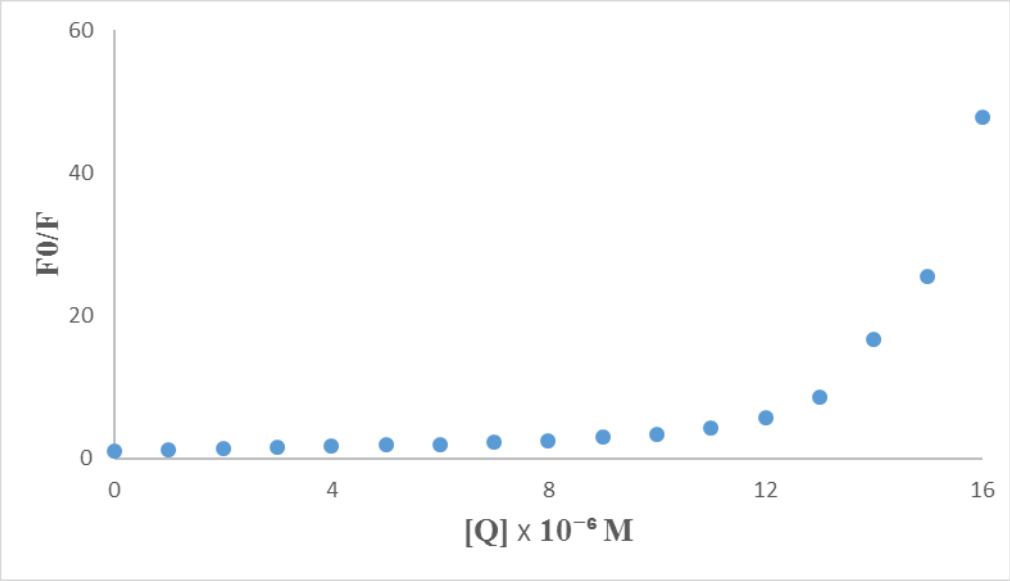


SI 7h. Stern-Volmer plot for quenching of HSA (15 μM) fluorescence by **3** at different concentrations ($\lambda_{ex}$ = 280 nm, $\lambda_{em}$ = 345 nm).

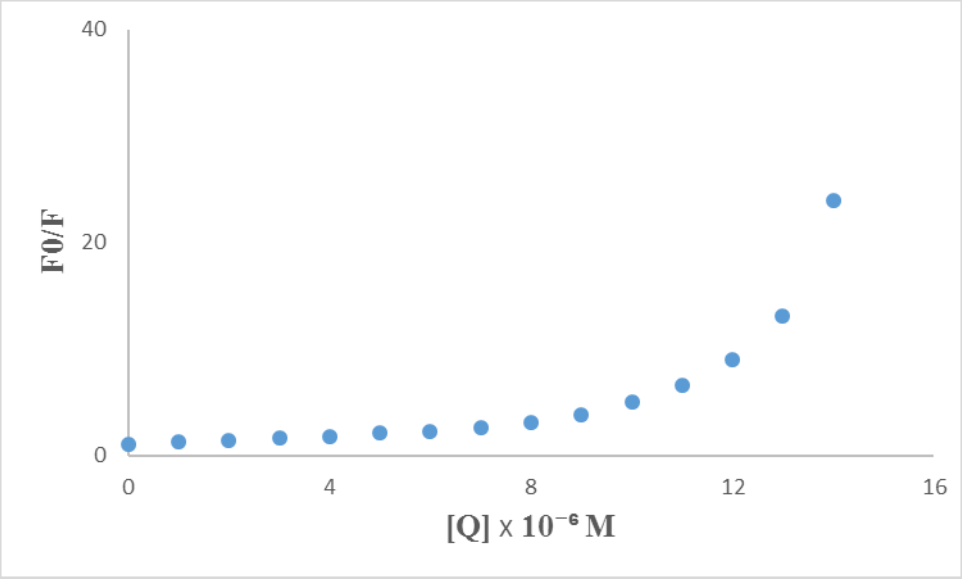


SI 7i. Stern-Volmer plot for quenching of HSA (15 μM) fluorescence by **4** at different concentrations ($\lambda_{ex}$ = 280 nm, $\lambda_{em}$ = 344 nm).

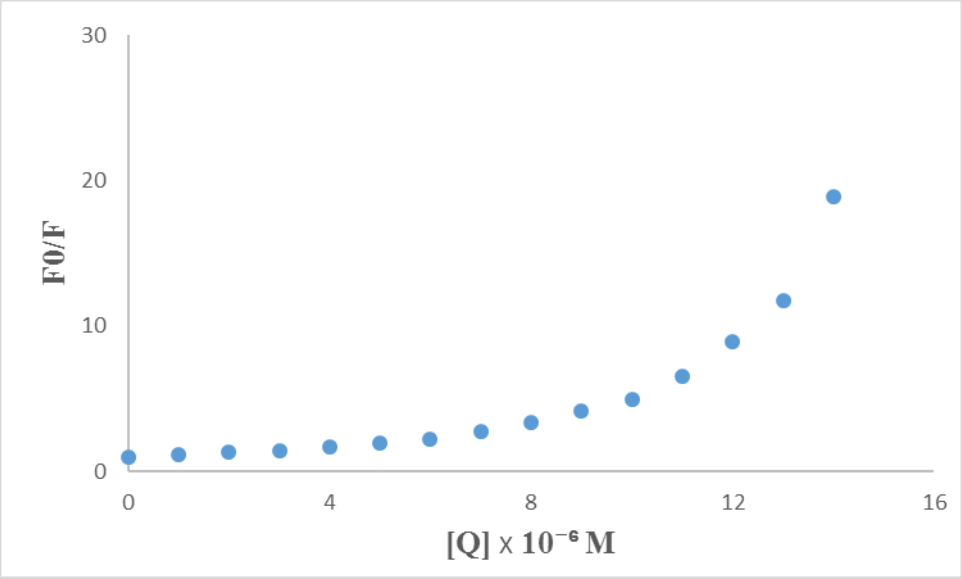


SI 7j. Stern-Volmer plot for quenching of HSA (15 μM) fluorescence by **5** at different concentrations ($\lambda_{ex}$ = 280 nm, $\lambda_{em}$ = 344 nm).

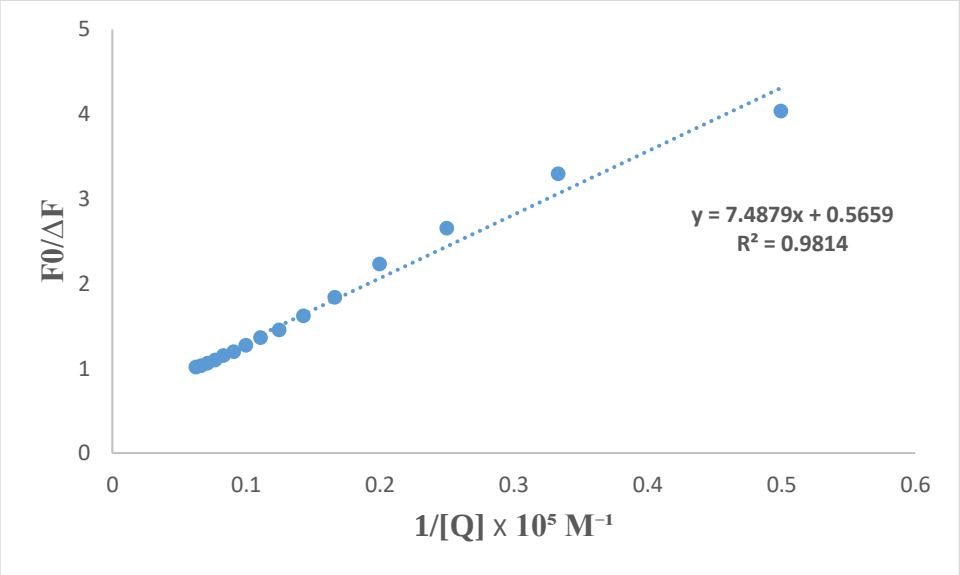


SI 7k. Plot of $\frac{F_0}{F_0 - F}$ *vs* 1/[L$^-$] for HSA in the presence of increasing concentrations of **1** at T = 298 K ($\lambda_{ex}$ = 280 nm, $\lambda_{em}$ = 344 nm).

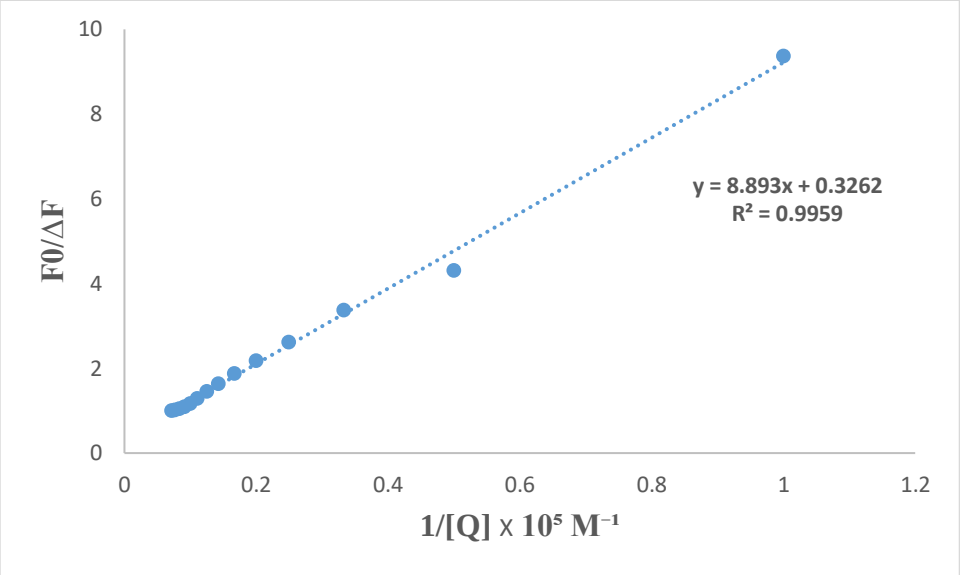


SI 7l. Plot of $\frac{F_0}{F_0 - F}$ *vs* 1/[L$^-$] for HSA in the presence of increasing concentrations of **2** at T = 298 K ($\lambda_{ex}$ = 280 nm, $\lambda_{em}$ = 347 nm).

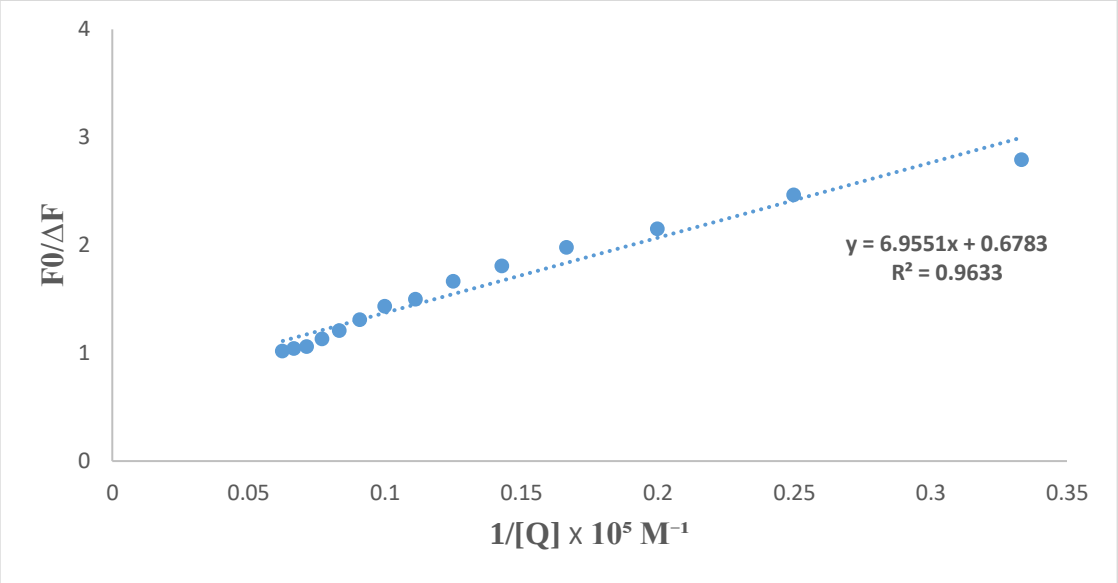


SI 7m. Plot of $\frac{F_0}{F_0 - F}$ *vs* 1/[L$^-$] for HSA in the presence of increasing concentrations of **3** at T = 298 K ($\lambda_{ex}$ = 280 nm, $\lambda_{em}$ = 345 nm).

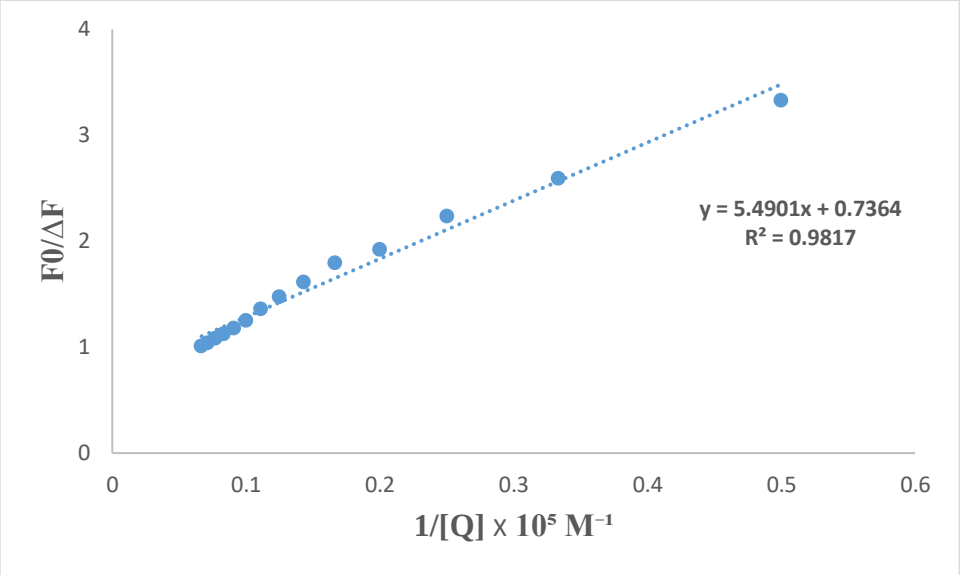


SI 7n. Plot of $\frac{F_0}{F_0 - F}$ *vs* 1/[L$^-$] for HSA in the presence of increasing concentrations of **4** at T = 298 K ($\lambda_{ex}$ = 280 nm, $\lambda_{em}$ = 344 nm).

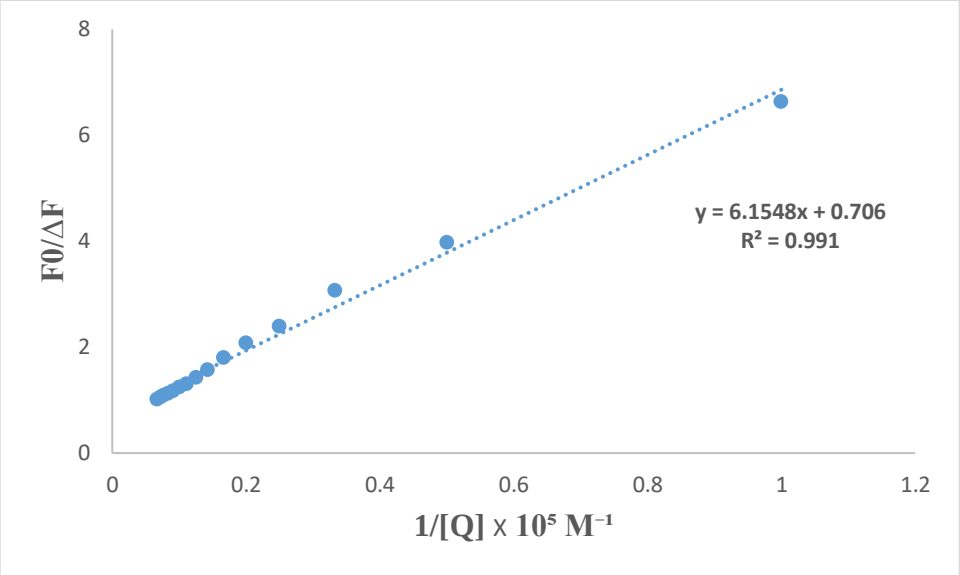


SI 7o. Plot of $\frac{F_0}{F_0 - F}$ *vs* 1/[L$^-$] for HSA in the presence of increasing concentrations of **5** at T = 298 K ($\lambda_{ex}$ = 280 nm, $\lambda_{em}$ = 344 nm).

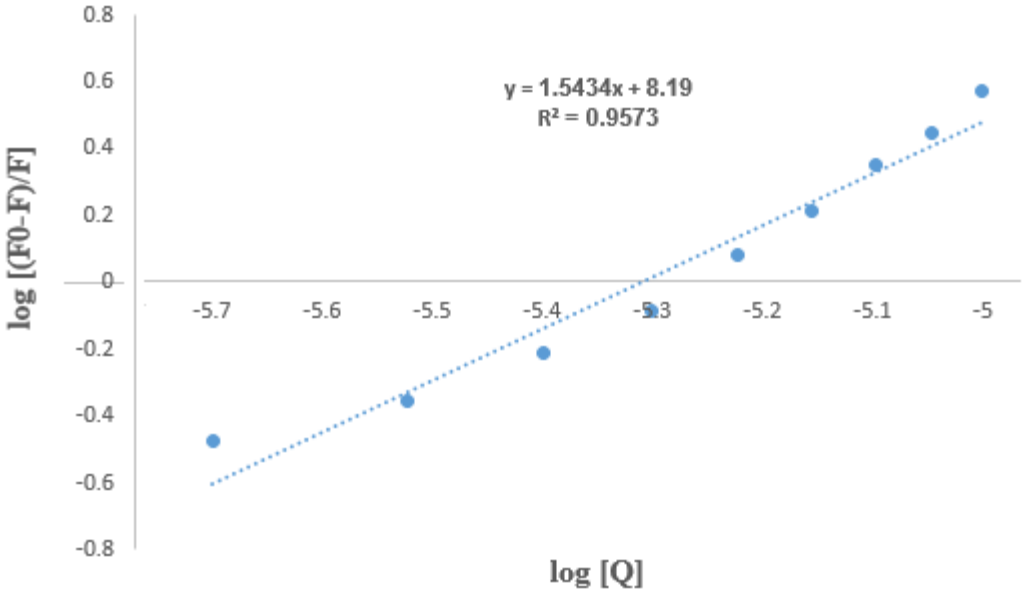


SI 7p. Double-log plots for the fluorescence quenching of the HSA by **1**.

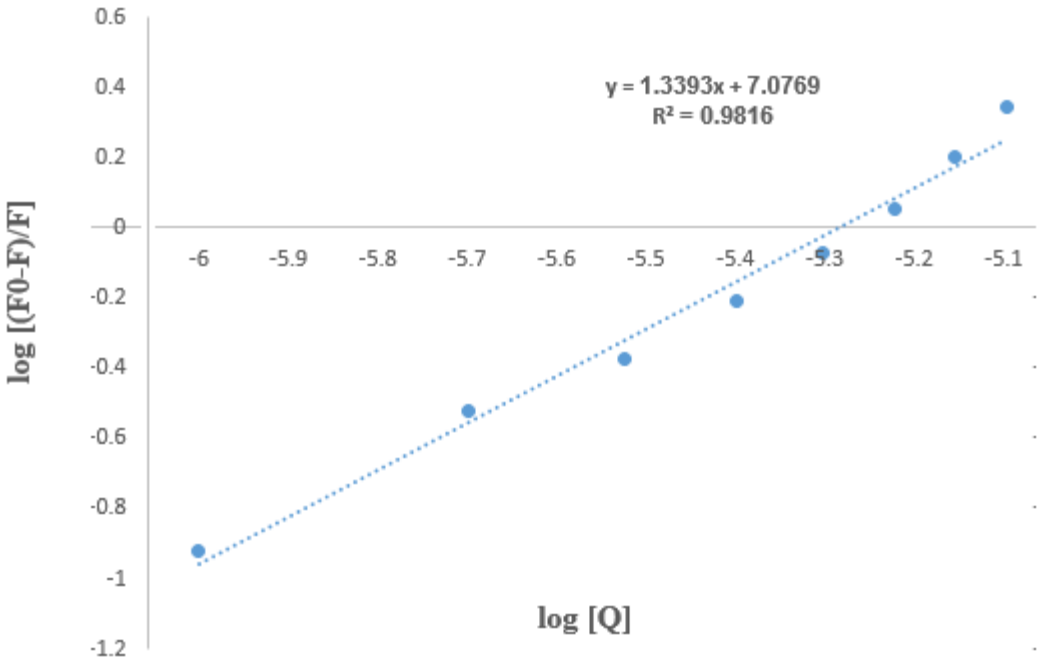


SI 7q. Double-log plots for the fluorescence quenching of the HSA by **2**.

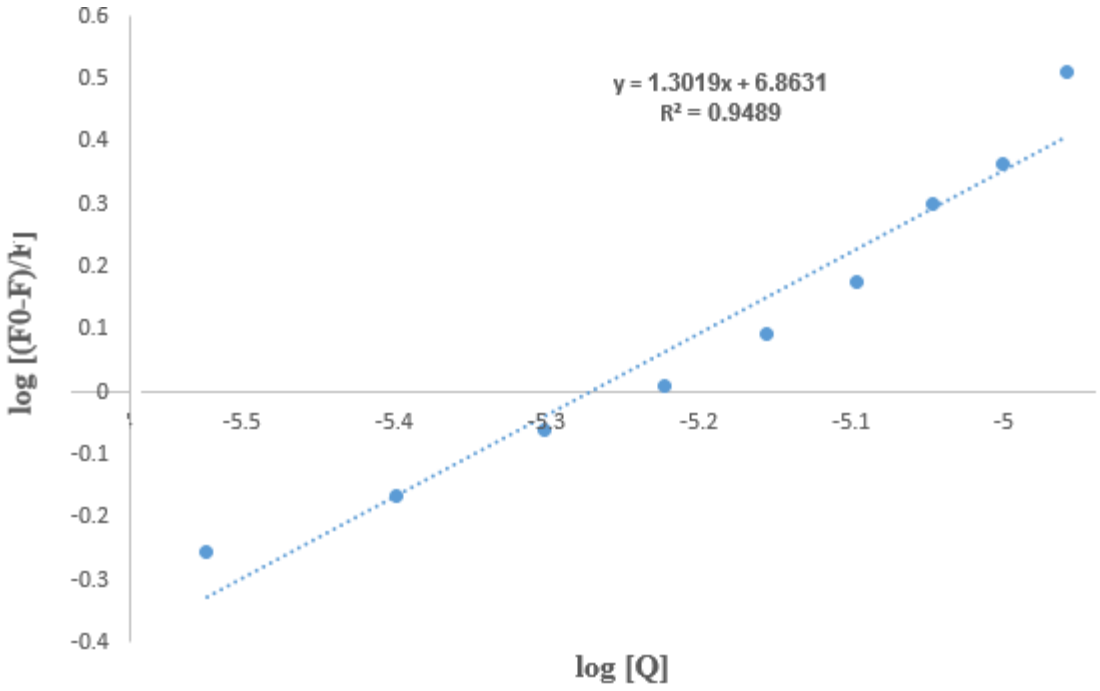


SI 7r. Double-log plots for the fluorescence quenching of the HSA by **3**.

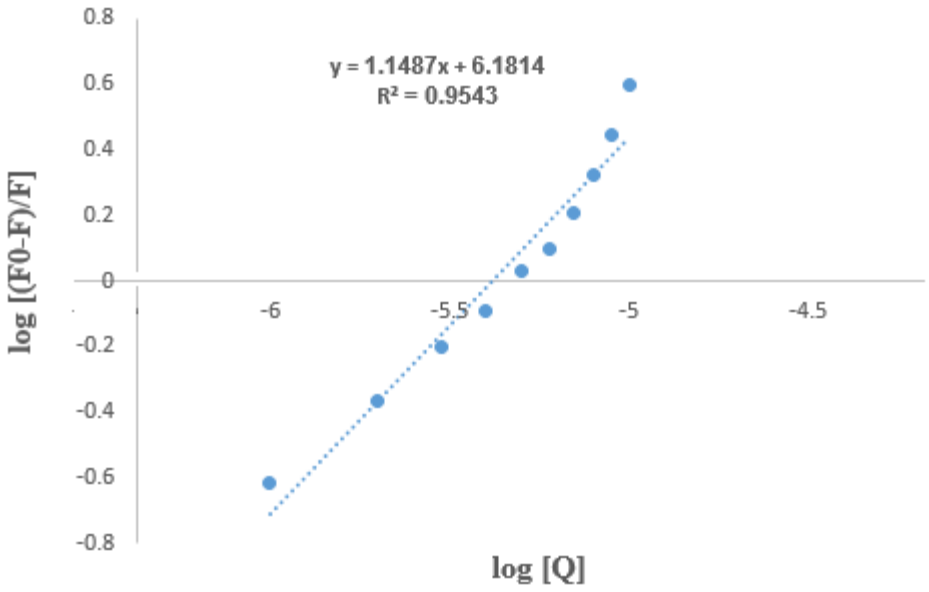


SI 7s. Double-log plots for the fluorescence quenching of the HSA by **4**.

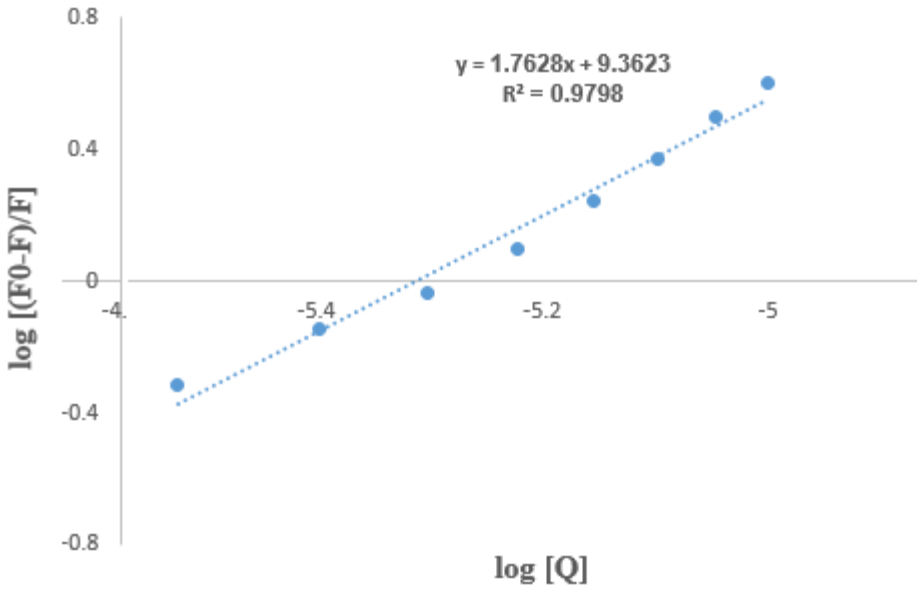


SI 7t. Double-log plots for the fluorescence quenching of the HSA by **5**.